Imperial College London
Consultants

IMPROVED PERFORMANCE OF LEAN-BURN COMBUSTION SEVENTH AND FINAL REPORT

Report reference: N62558-02-C-9011 R&D 9245-AN-01
Date: April 2003

A final report for
United States Army, European Research Office

Prepared by
Professor R.P. Lindstedt and Professor J.H. Whitelaw

On behalf of
IC Consultants Ltd

Problem Solving • Scientific Services • Expert Advice

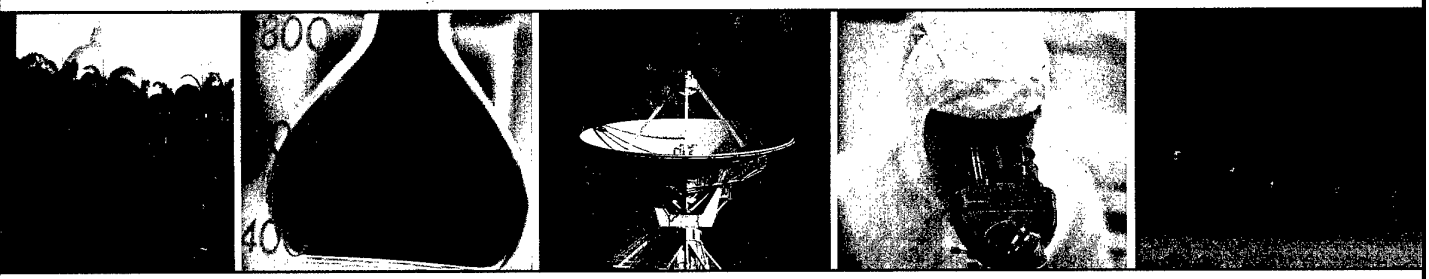

REPORT DOCUMENTATION PAGE

Form Approved
OMB No. 0704-0188

1. AGENCY USE ONLY *(Leave blank)*	2. REPORT DATE	3. REPORT TYPE AND DATES COVERED
	27 JAN 04	FINAL REPORT APRIL 2003

4. TITLE AND SUBTITLE
IMPROVED PERFORMANCE OF LEAN-BURN COMBUSTION
SEVENTH AND FINAL REPORT

5. FUNDING NUMBERS
9425-AN-01
N62558-02-C-9011

6. AUTHOR(S)
PROFESSOR R.P. LINDSTEDT
PROFESSOR J.H. WHITELAW

7. PERFORMING ORGANIZATION NAME(S) AND ADDRESS(ES)

8. PERFORMING ORGANIZATION REPORT NUMBER

9. SPONSORING / MONITORING AGENCY NAME(S) AND ADDRESS(ES)
U.S. ARMY - EUROPEAN RESEARCH OFFICE
EDISON HOUSE
223 OLD MARYLEBONE ROAD
LONDON NW1 5TH
UNITED KINGDOM

10. SPONSORING / MONITORING AGENCY REPORT NUMBER

11. SUPPLEMENTARY NOTES

12a. DISTRIBUTION / AVAILABILITY STATEMENT
APPROVED FOR PUBLIC DISTRIBUTION
DISTRIBUTION UNLIMITED
FINAL REPORT

12b. DISTRIBUTION CODE

13. ABSTRACT *(Maximum 200 words)*

14. SUBJECT TERMS
COMBUSTION, REACTANTS, THERMOCHEMISTRY

15. NUMBER OF PAGES
32

16. PRICE CODE

17. SECURITY CLASSIFICATION OF REPORT	18. SECURITY CLASSIFICATION OF THIS PAGE	19. SECURITY CLASSIFICATION OF ABSTRACT	20. LIMITATION OF ABSTRACT
UNCLASSIFIED	UNCLASSIFIED	UNCLASSIFIED	

IMPROVED PERFORMANCE OF LEAN-BURN COMBUSTION

Seventh and Final Report

R P Lindstedt and J H Whitelaw
Imperial College
London SW7 2BX

United States Army, European Research Office
Contract N62558-02-C-9011
April 2003

SUMMARY

The focus of the research described here is on establishing and controlling the causes of combustion instabilities in fuel lean combustion systems. The frequencies of the dominant instability modes are typically < 500 Hz and a comprehensive closure at second moment level, which accounts for the effects of persistent non-gradient transport in a consistent manner, has been applied to compute the combusting flow characteristics in the plane duct configuration of De Zilwa et al (2001). Results indicate that aerodynamic strain and the treatment of pressure related terms have a major impact under stable and oscillating combustion conditions and a consistent first order redistribution model has been derived and applied. The calculations indicate that the treatment of the duct exit boundary condition is critical in the context of the distribution of energy between different acoustic modes. An investigation into alternative boundary treatments for time-dependent flows suggests that the most appropriate technique for reproducing experimental impedances is to extend the computational domain to include the induced flow outside the duct. The calculation method is shown to represent combustion of methane and air at equivalence ratios that give rise to stable combustion and the low-amplitude oscillations that exit at low Reynolds numbers and equivalence ratios between lean extinction and the lean stability limit.

Experiments have been performed with methane, propane and ethylene fuels, premixed with air and include the determination of flammability and stability limits with hot and cold ducts, the nature of combustion instabilities and some aspects of control. They fulfil the obligations of the contract and provide information that has and will continue to assist the development of the above computer method. They show, for example, that ethylene-air mixtures had the highest flame speed for any given equivalence ratio while methane had the slowest and this was reflected in the wider flammability and stability limits of ethylene. Increase in the downstream wall temperature allowed partial pre-heat of the mixture as it flowed past the step, increasing the flame speed and widening the flammability limits but not the region of high amplitude acoustic oscillations. Passive control with fuel injection was demonstrated at lean and stoichiometric conditions, but within narrow intervals of operation for each condition and further research is required to optimize important parameters such as injector to step separation, injection flow rate and injector mixture equivalence ratio for a range of Reynolds numbers and equivalence ratios. Passive acoustic control was also demonstrated over a range of frequencies and proved most effective at the second harmonic of the duct, while active control produced better results at half this value.

INTRODUCTION

The combustion of lean mixtures of air and natural gas can lead to low emissions of nitrous oxides but with the possibility of unstable combustion leading to increased emissions of carbon monoxide and hydrocarbons. Indeed, it has been shown that the oscillations can also lead to increased concentrations of nitrous oxides particularly as extinction is approached. The research described here brings together calculation and experimental methods to represent the physical phenomena and to determine ways in which to allow the combustion of lean mixtures without the related disadvantages. It stems from experiments by De Zilwa et al (2000, 2001) who showed that the unsteady combustion found close to the lean extinction limit was due in part to poor flame stabilisation and a process of extinction and re-light. The overall result was amplitude and frequency modulated oscillations at frequencies that increased with flow rate and heat-release rate. The latter is strongly dependent upon the local stoichiometry of the mixture and the amplitudes can be greatly increased by coupling with acoustic oscillations. The combination of the two sources of oscillation can make control difficult.

Ad hoc testing involves geometric changes and is necessarily limited so that a calculation method has been developed to represent the physical phenomena and, in conjunction with new experiments, to determine the preferred methods of control and the resulting control performance. The focus here is on the coupling of dominant lower frequency modes (< 500 Hz) with heat release in premixed or partially premixed combustion devices. The latter burning mode may arise, for example, through the stabilization of combustion thorough diffusion flame pilots. A key feature is the provision of accurate predictions of the dynamic behaviour of turbulent flames and the associated development of consistent flux- and combustion-related model elements by Lindstedt and Vaos (1999) and Kuan and Lindstedt (2002). An issue of particular importance arises in the context of the treatment of turbulent fluxes that readily become dominated by pressure gradient terms and a consistent treatment thus requires a coupling to the heat release. Given the low frequencies of the dominant instability modes, a comprehensive closure at second moment level, which accounts for the effects of pressure gradients in a consistent manner, is at present an obvious choice given the presence of persistent non-gradient transport in several regimes of premixed turbulent combustion. In addition to the time-dependent compressible Navier-Stokes equations, transport equations for the Reynolds stresses, scalar fluxes and scalar quantities (e.g. species concentrations) are therefore also required. The approach is used here in the context of modest deviations from the high Damköhler limit and progress with respect to the inclusion of transport equations for joint probability density functions into time-dependent hybrid calculation procedures is also outlined. The burning properties applied in the context of the high Damköhler approaches have been derived on the basis of the simulation of strained steady state and transient flames which are computed on the basis of comprehensively validated detailed chemical kinetics, for example by Lindstedt (1998) and Lindstedt and Skevis (2000).

This final report is presented in two sections dealing respectively with the development and use of the calculation method and experiments that supplement and complement those of Emiris and Whitelaw (2002, 2003). It corresponds to a two-year program necessarily truncated by three months.

PART 1: CALCULATIONS

An existing computer code has been formulated to represent the isothermal and chemically reacting configurations of De Zilwa et al (2001). The cases featuring combustion of methane and air at equivalence ratios that give rise to stable and unstable combustion are considered with the main emphasis on the latter. Results have been obtained with both eddy viscosity and full second moment closures and show that experimental data can be reproduced with encouraging accuracy for both non-reactive and reactive cases (Task 1 of the proposal). The results indicate that strain effects and terms related to pressure gradients exert a major influence and the thermochemical closure has accordingly been extended by the introduction of strain functions based on Markstein lengths. The latter have been determined through numerical simulations, featuring comprehensive detailed chemistry, of steady

counterflow flames as well as transient spherical flame kernels. The current procedure allows the relevance of a range of different definitions to be explored through the tracking of arbitrary isotherms as well as use of integral properties. Improved models for pressure terms related to redistribution modelling have also been derived and the resulting improvements of the calculation procedure (Task 3) have been implemented to examine the unsteady flows experienced close to the lean limit and to represent the observed phenomenon of extinction and re-light (Task 4). In an extension of the work, the latter phenomena have been studied in bluff body stabilised flames through the application of time-dependent transported PDF simulations featuring a hybrid stochastic and finite volume approach. The developed calculation methods permit the introduction of local fuel injection and diffusion flame type pilots with increasing thermochemical accuracy and effectively fulfil the requirements of Task 6 though the evaluation against the experimental data procured by Emiris and Whitelaw (2002,2003) remains to be performed. The extension of the calculation method to permit unsteady fuel injection (Task 8) has, however, been completed. This first part of the report has been prepared in 6 sections dealing respectively with the conservation equations, thermochemistry, the numerical procedure, results, effects of boundary conditions and conclusions.

CONSERVATION EQUATIONS FOR PREMIXED REACTANTS

The aerothermochemical fields are governed by the conservation equations for mass, momentum and scalars cast in a density-weighted form. Laminar diffusion terms and external force fields are neglected.

(1) $$\frac{\partial \bar{\rho}}{\partial t}+\frac{\partial \bar{\rho}\tilde{u}_l}{\partial x_l}=0$$

(2) $$\frac{\partial \bar{\rho}\tilde{u}_i}{\partial t}+\frac{\partial \bar{\rho}\tilde{u}_l\tilde{u}_i}{\partial x_l}=-\frac{\partial \bar{p}}{\partial x_i}-\frac{\partial \bar{\rho}\widetilde{u_i''u_l''}}{\partial x_l}$$

(3) $$\frac{\partial \bar{\rho}\tilde{c}}{\partial t}+\frac{\partial \bar{\rho}\tilde{u}_l\tilde{c}}{\partial x_l}=-\frac{\partial \bar{\rho}\widetilde{u_l''c''}}{\partial x_l}+\bar{S}_c$$

In the context of time dependent flows, it is important to note that changes in the velocity and scalar fields drive the generation of turbulence and that the feedback is provided though the turbulent correlation terms on the RHS of equations (2,3). The latter are here treated through the corresponding transport equations for the Reynolds stresses (4-6) and scalar fluxes (7-8).

(4) $$\frac{\partial \bar{\rho}\widetilde{u_i''u_j''}}{\partial t}+\frac{\partial \bar{\rho}\tilde{u}_l\widetilde{u_i''u_j''}}{\partial x_l}=\frac{\partial T_{ijl}}{\partial x_l}+P_{ij}+\Phi_{ij}+\phi_{ij}-\bar{\rho}\varepsilon_{ij}$$

The terms on the RHS represent, in order, turbulent transport of the Reynolds stresses, effects of mean strain (or "production" P_{ij}), effects of mean pressure gradients (Φ_{ij}), the turbulent pressure strain term (ϕ_{ij}) and viscous dissipation ($\rho\varepsilon_{ij}$). Turbulent premixed combustion in ducts is subject to imposed pressure gradients which induce strong modifications to the flame structures due to the resulting preferential acceleration of heavy cold fresh and light hot burnt gases. Pressure gradient effects are thus expected to dominate turbulence production, destruction and redistribution. The treatment of such terms is exceedingly difficult in combusting flows and the situation is further complicated if the time-dependent equations are used to resolve the lower frequencies of the turbulence spectrum as the need arises for the matching to the (modeled) solutions for the unresolved higher frequencies.

(5,6) $$P_{ij}=-\bar{\rho}\left[\widetilde{u_i''u_l''}\frac{\partial\tilde{u}_j}{\partial x_l}+\widetilde{u_j''u_l''}\frac{\partial\tilde{u}_i}{\partial x_l}\right]\quad \Phi_{ij}=-\left[\overline{u_i''}\frac{\partial \bar{p}}{\partial x_j}+\overline{u_j''}\frac{\partial \bar{p}}{\partial x_i}\right]\quad \phi_{ij}=-\left[\overline{u_i''\frac{\partial p'}{\partial x_j}}+\overline{u_j''\frac{\partial p'}{\partial x_i}}\right]$$

The modelling of the pressure correlation terms in the Reynolds stress equations is the focal point of second moment closures. They can be decomposed into redistributive and isotropic parts and the latter may be further split into pressure transport and pressure dilation terms. Details have been reported by Lindstedt and Vaos 1999. Redistribution terms are invariably modelled by recasting closures (derived on a constant density basis) in a density weighted form and a similar procedure is applied to the pressure scrambling terms. An algebraic expression for the density-weighted fluctuations, which forms part of the mean pressure gradient term, can be derived and the corresponding scalar fluxes for the reaction progress variable are given below.

(7) $$\frac{\partial \bar{\rho}\widetilde{u_i''c''}}{\partial t}+\frac{\partial \bar{\rho}\widetilde{u}_l\widetilde{u_i''c''}}{\partial x_l}=\frac{\partial T_{ilc}}{\partial x_l}+P_{ic}+\Phi_{ic}+\phi_{ic}+\overline{u_i''S_c}-\rho\varepsilon_{ic}$$

(8) $$P_{ic}=-\bar{\rho}\left[\widetilde{u_l''c''}\frac{\partial \widetilde{u}_i}{\partial x_l}+\widetilde{u_i''u_l''}\frac{\partial \widetilde{c}}{\partial x_l}\right] \quad \Phi_{ic}=-\overline{c''}\frac{\partial \bar{p}}{\partial x_i} \quad \phi_{ic}=-\overline{c''\frac{\partial p'}{\partial x_i}}$$

The treatment of the pressure strain terms features a rearrangement into redistributive and isotropic parts with the latter decomposed into pressure transport and dilatation terms.

(9) $$\phi_{ij}^R=-\left[\overline{u_i''\frac{\partial p'}{\partial x_j}}+\overline{u_j''\frac{\partial p'}{\partial x_i}}-\frac{2}{3}\delta_{ij}\overline{u_l''\frac{\partial p'}{\partial x_l}}\right] \quad \phi_{ij}^T=-\left[\frac{2}{3}\delta_{ij}\overline{\frac{\partial p'u_l''}{\partial x_l}}\right] \quad \phi_{ij}^D=\left[\frac{2}{3}\delta_{ij}\overline{p'\frac{\partial u_l''}{\partial x_l}}\right]$$

The corresponding pressure strain term in the scalar flux equation may be recast in terms of pressure transport (T) and scrambling (S) terms.

(10,11) $$\phi_{ic}^T=-\frac{\overline{\partial p'c''}}{\partial x_i} \quad \text{and} \quad \phi_{ic}^S=-\overline{p'\frac{\partial c''}{\partial x_i}}$$

The specific model expressions applied are described below. The "return to isotropy" and "strain" redistribution parts are obtained from model formulations derived in non-reacting flows. Several suggestions exist at various levels of complexity and the Generalized Langevin (Haworth and Pope 1986) and SSG (Speziale et al 1991) forms have been considered. An important feature of the current work is that is that a consistent closure for the pressure scrambling term in the scalar flux equation is required in a manner that allows for realizable modelling of both pressure strain correlations. The "return" and "strain" redistribution parts take the following equivalent forms where **b** denotes the anisotropy tensor. The superscript "CD" indicates the constant density origin of the model.

(12) $$\phi_{ij}^{CD}=\bar{\rho}\left[\frac{\tilde{\varepsilon}}{\tilde{k}}C_{ij}[\mathbf{b}]+B_{ijkl}[\mathbf{b}]\frac{\partial \widetilde{u}_k}{\partial x_l}\right]\tilde{k}=\bar{\rho}G_{ik}\widetilde{u_k''u_j''}+\bar{\rho}G_{jk}\widetilde{u_k''u_i''}+\bar{\rho}(C_o+\frac{2}{3})\delta_{ij}\tilde{\varepsilon}$$

The corresponding model form for the scalar flux equation is

(13) $$\phi_{ic}^{CD}=\bar{\rho}\left[\frac{\tilde{\varepsilon}}{\tilde{k}}C_{ij}^c[\mathbf{b}]+B_{ijkl}^c[\mathbf{b}]\frac{\partial \widetilde{u}_k}{\partial x_l}\right]\widetilde{u_j''c''}=\bar{\rho}G_{ik}\widetilde{u_k''c''}-\bar{\rho}\frac{\tilde{\varepsilon}_c}{\widetilde{c''^2}}\widetilde{u_i''c''}$$

In Eq. (13) the constant C_0 is assigned the value 2.1. The functional form for G_{ij} depends on the specific closure adopted and details are available elsewhere (e.g. Lindstedt and Vaos 1999). In turbulent premixed flames the "production" by strain is not the principal cause of anisotropy. Therefore, it has been pointed out (Lindstedt and Vaos 1998) that regardless of specific model formulations the rate at which energy is transferred between components is substantially lower than the rate at which anisotropy is produced. Model formulations for redistribution should therefore explicitly

include an additional part that represents preferential acceleration effects and a further indication comes from the Poisson equation for the fluctuating pressure given below.

$$\frac{1}{\rho}\frac{\partial^2 p'}{\partial x_j^2} = -\frac{\partial^2}{\partial x_i \partial x_k}\left(u_i'u_k' - \overline{u_i'u_k'}\right) - 2\frac{\partial^2 U_k}{\partial x_i}\frac{\partial u_j'}{\partial x_k} + \frac{\partial f_i'}{\partial x_i}$$

The above equation can be solved using Green's function for points remote from the flow boundary and substituting for the fluctuating pressure gives the following expression for the pressure strain term.

$$\begin{aligned}\phi_{ij} = &-\frac{1}{4\pi}\int_V \left[\frac{\partial^3 \overline{u_k' u_l' u_i'}}{\partial x_l \partial x_k \partial x_j} + \frac{\partial^3 \overline{u_k' u_l' u_j'}}{\partial x_l \partial x_k \partial x_i}\right]\frac{dV}{|\underline{x}' - \underline{x}|} \\ &-\frac{1}{2\pi}\int_V \frac{\partial U_k}{\partial x_i}\left[\frac{\partial^2 \overline{u_l' u_i'}}{\partial x_k \partial x_j} + \frac{\partial^2 \overline{u_l' u_j'}}{\partial x_k \partial x_i}\right]\frac{dV}{|\underline{x}' - \underline{x}|} \\ &+\frac{1}{4\pi}\int_V \left[\frac{\partial^2 \overline{u_i' f_l'}}{\partial x_l \partial x_j} + \frac{\partial^2 \overline{u_j' f_l'}}{\partial x_l \partial x_i}\right]\frac{dV}{|\underline{x}' - \underline{x}|}\end{aligned}$$

In the above equation f denotes an external force acting on the fluid. The expression suggests that the pressure strain term consists of three parts; a "slow" part, which will be referred to as "return to isotropy," and two "rapid" parts, one associated with strain and the other, with the external force. Preferential acceleration effects by the mean pressure gradient can be seen in the same light as the application of an external force on the fluid. Indeed, it is difficult to distinguish between effects induced by acceleration due to pressure gradient or external force fields (e.g. gravity) since both are linearly superimposed in the momentum equation. The response of turbulence to both acceleration vectors may therefore be expected to be identical.

The acceleration redistribution/scrambling parts should obviously have a tensorial form as single term invariant "corrections" would result in a non-traceless redistribution term. The following functional forms are used.

(14) $$\phi_{ij}^R = \phi_{ij}^{CD} + \phi_{ij}^A \quad \text{where} \quad \phi_{ij}^A = -\left[A_{jk}^i[b,\overline{u}''] + A_{ik}^j[b,\overline{u}'']\right]\rho a_k$$

(15) $$\phi_{ic}^R = \phi_{ic}^{CD} + \phi_{ic}^A \quad \text{where} \quad \phi_{ic}^A = -A_{ik}[b,\overline{u}'',\overline{c}'']\rho a_k \quad \text{and} \quad a_k = -\frac{1}{\overline{\rho}}\frac{\partial \overline{p}}{\partial x_k}$$

The Cayley-Hamilton theorem states that the most general form involving the anisotropy tensor should include terms up to the second order. However, such models can ill-behave near one- and two-component states of turbulence due to the imposition of realizability constraints on second order non-linear terms (Speziale et al 1993). Furthermore, such models are invariably complex (e.g. Shih and Lumley 1985 and Lindstedt and Vaos 1999) and their application even to simple steady flows can be problematic. The zeroth order approximation is commonly known as the IP (Isotropization of Production) model and has been used in modelling buoyant flows (e.g. Gibson and Launder 1978). To date, only zeroth order models have been considered in combustion applications (Lindstedt and Vaos 1998, 1999), but given the importance of such terms in the current flows a first order model has been formulated. Neglecting second order anisotropic terms, the general form for the A_{jk}^i tensor can be written as:

(16) $$\begin{aligned}A_{jk}^i = &f_1\delta_{jk}\,\widetilde{u_i''c''} + f_2\left(\delta_{ik}\,\widetilde{u_j''c''} + \delta_{ij}\,\widetilde{u_k''c''}\right) + f_3 b_{jk}\,\widetilde{u_i''c''} + f_4\left(b_{ik}\,\widetilde{u_j''c''} + b_{ij}\,\widetilde{u_k''c''}\right) \\ &+ f_5\delta_{jk}\,b_{mi}\,\widetilde{u_m''c''} + f_6\,\widetilde{u_m''c''}\left(\delta_{ik}b_{mk} + \delta_{ij}b_{mi}\right)\end{aligned}$$

Application of realizability ($A^{i}_{\alpha k} \to 0$ as $\widetilde{u''^2_\alpha} \to 0$) constraints and contraction (A^i_{jk} is traceless) yields the following values for the six coefficients of the linear model.

$$f_1 = 0.4 \qquad f_2 = -0.1 \qquad f_3 = 0.1$$
$$f_4 = -0.3 \qquad f_5 = 0.1 \qquad f_6 = 0.0$$

Introduction of the bimodal PDF assumption, the reaction progress variable and the expansion ratio yields the following relationships.

(17) $$\overline{u''_i} = \tau \frac{\overline{\rho}}{\rho_u} \widetilde{u''_i c''} \qquad \overline{c''} = \tau \frac{\overline{\rho}}{\rho_u} \widetilde{c''^2} \qquad \beta_i = \tau \frac{\overline{\rho}}{\rho_u} \frac{\partial \overline{P}}{\partial x_i}$$

Accordingly, a first order model for the "rapid pressure" term can be written as

(18) $$\phi^{\wedge}_{ij} = -0.3\left(\Phi_{ij} - \frac{1}{3}\delta_{jk}\Phi_{kk}\right) + 0.3\Phi_{kk}\, b_{ij} - 0.2\beta_k\left(\widetilde{u''_j c''}\, b_{ik} + \widetilde{u''_i c''}\, b_{jk}\right) + 0.2\beta_j\, \widetilde{u''_k c''}\, b_{ik} + 0.2\beta_i\, \widetilde{u''_k c''}\, b_{jk}$$

The corresponding expression for the IP model is given below and, although the value of C_{AR} for the model to be traceless is 0.3, a value of 0.5 has been used in buoyant flow calculations (Gibson and Launder 1978).

(19) $$\phi^{\wedge}_{ij} = -C_{AR}\left(\Phi_{ij} - \frac{1}{3}\delta_{jk}\Phi_{kk}\right)$$

The corresponding model for the scalar flux equation can be formulated using the same approach. Again, neglecting second order terms, the general model for A_{ik} can be written as

(20) $$A_{ik} = \alpha_1 \widetilde{c''^2}\,\delta_{jk} + \alpha_2 \widetilde{c''^2}\, b_{ik}$$

Applying realizability and contraction constraints results in the following zeroth (21) and first (22) order models for $\phi^{\wedge}_{ic}$.

(21,22) $$\phi^{\wedge}_{ic} = C_{AS}\widetilde{c''^2}\,\beta_i \qquad \phi^{\wedge}_{ic} = \frac{1}{3}\widetilde{c''^2}\,\beta_i - \widetilde{c''^2}\, b_{ik}\beta_k$$

A value of C_{AS} value of 1/3 needed for the term to be traceless and the behaviour of the zeroth order models has been evaluated in the context of premixed turbulent flames (Lindstedt and Vaos 1999) and shown to yield encouraging results.

A number of closures have been suggested for the triple moments. However, the contributions of the diffusion terms to the overall budget of the Reynolds stresses and scalar fluxes is moderate and, consequently, the turbulent transport of the second moments is here modelled using a generalized gradient diffusion model.

(23,24) $$\frac{\partial T_{ijl}}{\partial x_l} + \phi^T_{ij} = \frac{\partial}{\partial x_k}\left[C_s \overline{\rho}\frac{\tilde{k}}{\tilde{\varepsilon}} \widetilde{u''_k u''_l} \frac{\partial \widetilde{u''_i u''_j}}{\partial x_l}\right] \qquad \frac{\partial T_{ilc}}{\partial x_l} + \phi^T_{ic} = \frac{\partial}{\partial x_k}\left[C_s \overline{\rho}\frac{\tilde{k}}{\tilde{\varepsilon}} \widetilde{u''_k u''_l} \frac{\partial \widetilde{u''_i c''}}{\partial x_l}\right]$$

The closure for the dissipation rate of the turbulent kinetic energy is obtained by the standard variable density transport equation model. The thermodynamic properties are evaluated from JANAF polynomials and the temperature is calculated via Newton iteration.

THERMOCHEMISTRY

The closure for the chemical source term presents an interesting problem that entails the determination of an appropriate time scale for scalar turbulence. Traditionally, the closure for the scalar dissipation rate in the high Damköhler number regime is based on a constant timescale ratio leading to a direct

relation to the mechanical time scale. It has been shown by Lindstedt and Vaos (1999), based on a fractal analysis, that the time scale ratio in the former regime needs to be modified to account for flame propagation. Bray et al (2001) have recently evaluated a number of reaction rate closures in the context of the opposed jet geometry. The conclusions are interesting and suggest that reaction rate closures typically fail to predict qualitative trends correctly. Furthermore, it was shown that, irrespective of the level of closure adopted – algebraic or transport equation based – current models could usually not be calibrated to perform satisfactorily irrespective of the choice of modelling constants. The exception was the fractal based closure (25) though it must be recognized that the uncertainty relating to the modelling constant remains.

$$\bar{S}_c = \bar{\rho} C_R \frac{\tilde{\varepsilon}_c}{\tilde{c''^2}} \tilde{c}(1-\tilde{c}) \cong \bar{\rho}_o C_R \left[\frac{u_l}{v_k}\right] \frac{\tilde{\varepsilon}}{\tilde{k}} \tilde{c}(1-\tilde{c}) \tag{25}$$

Kuan et al (2002) extended the above closure to strongly turbulent flows and showed that the model could reproduce explosion kernels with overpressures in excess of 160 kPa.

$$\bar{S}_c = \bar{\rho} C_R \left[1 + C_R^* \frac{\bar{\rho}_o}{\bar{\rho}} \frac{u_l}{v_k}\right] \frac{\tilde{\varepsilon}}{\tilde{k}} \tilde{c}(1-\tilde{c}) \tag{26}$$

The two expressions ($C_R \sim 3$ and $C^*_R \sim 1$) are here referred to as the lower (25) and upper (26) limits given their past application. The limitations underlying the derivations of the above expressions are obvious but to a large degree identical to those present in standard modelling approaches. From a practical perspective, however, the derived form shown below ensures consistent scaling behaviour for turbulent burning velocities in the high Damköhler number regime of combustion. The velocity reaction rate correlation term is here closed through the assumption of a bimodal PDF.

$$-\bar{\rho} \frac{\tilde{\varepsilon}_c}{\tilde{c''^2}} \widetilde{u_i'' c''} + \overline{u_i'' S_c} = \frac{\bar{S}_c}{\tilde{c''^2}} \left(\frac{1}{2} - \tilde{c}\right) \tag{27}$$

Different models for the pressure dilation term have been proposed by Lindstedt and Hulek (1995) and Zhang and Rutland (1994). The former suggestion has the virtue of being consistent with the assumed thermochemical conditions and, while the latter is heuristic in nature, it does not present problems in terms of realizability. In the present work the term has been omitted.

DETERMINATION OF STRAIN FUNCTIONS

The laminar burning velocity features in both of the above (25,26) reaction rate expression and the expansion ratio appears in other terms (17). In order to improve the high Damköhler number based calculation procedure, the dependence of these properties upon the rate of strain need to be established. The improvements in the thermochemistry have been pursued through simulations performed in a Lagrangian frame of reference featuring comprehensively validated detailed chemistry (Lindstedt and Skevis 2000) and accurate transport algorithms. The form of the Lagrangian equations applied is given below (Lindstedt et al 1998).

$$\rho = \frac{1}{R^2} \frac{\partial M}{\partial R} \qquad u = \frac{dR}{dt}$$

$$\rho \frac{\partial Y_k}{\partial t} = -\rho \frac{\partial}{\partial M} \left\{R^2 \Im_k\right\} + R_k M_k \quad R_k = \sum_{j=1}^{N_{reac}} \Xi_{jk} \left[k_j^f \prod_{l=1}^{N_{sp}} \phi_l - k_j^r \prod_{l=1}^{N_{sp}} \phi_l\right]$$

$$\rho \frac{\partial h}{\partial t} = -\rho \frac{\partial}{\partial M} \left\{R^2 \Im_h\right\} + \rho \frac{\partial}{\partial M} \left\{\sum_{k=1}^{N_{sp}} R^2 h_k \left[-\Im_k + \Im_n\right]\right\}$$

The corresponding transport terms account for differential and thermal diffusion and the equation set is solved using a block implicit method with a second order convergence. The calculation method is currently second order accurate in time and space and features dynamic local grid refinement.

$$\Im_k = -\rho^2 D_k R^2 \left(\frac{\partial Y_k}{\partial M} - Y_k \frac{1}{n} \frac{\partial n}{\partial M} \right) - \rho W_k Y_k - \rho V_c Y_k \quad W_k = -\rho R^2 \frac{D_k \Theta_k}{x_k} \frac{1}{T} \frac{\partial T}{\partial M}$$

$$\Im_n = -\rho R^2 \frac{\lambda}{C_p} \frac{\partial Y_k}{\partial M}$$

$$\Im_h = -\rho R^2 \frac{\lambda}{C_p} \frac{\partial h}{\partial M} \quad V_c = \left[-\sum_{k=1}^{N_{sp}} \rho^2 D_k R^2 \left(\frac{\partial Y_k}{\partial M} - Y_k \frac{1}{n} \frac{\partial n}{\partial M} \right) + \rho W_k Y_k \right] \left(\sum_{k=1}^{N_{sp}} \rho Y_k \right)^{-1}$$

Transient flame simulations demand substantial computational resources despite the use of sophisticated fully implicit and locally adaptive solution algorithms. The computed results have been parameterized in terms of Markstein lengths corresponding to integral properties across the entire laminar flame structure. Integral properties are preferred as there is a direct relationship to the heat release rate and, therefore, to the ability to sustain combustion. The definition of the Markstein length given below is used here where a denotes the rate of strain.

$$L_{\text{int}} = \frac{u_l(0) - u_l(a)}{a}$$

The current initial pressure and temperature corresponds to ambient conditions though the approach can readily be extended to the high pressures and inlet temperatures associated with practical combustors. Parameters based on the tracking of isotherms and/or inner reference planes have also been extracted and shown to offer little in terms of a consistent modeling framework. The initial matrix of conditions (Stoichiometries: 0.50, 0.60, 0.80, 1.00, 1.10, 1.20, 1.40 and 1.60) is completed and results are given in Table 1.

ϕ	0.50	0.60	0.80	1.00	1.10	1.20	1.40	1.60
L_{int}	0.375	0.229	0.127	0.110	0.120	0.150	0.311	0.694

Table 1. Initial set of Markstein lengths (mm) obtained by evaluating the integral properties of transient flame kernels.

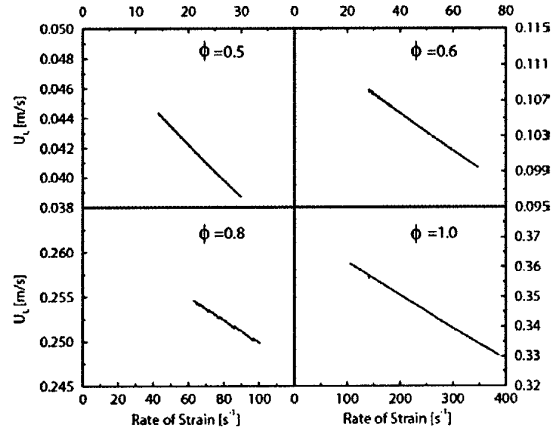

Figure 1. The response of the integral laminar burning velocity to the rate of strain as extracted from transient spherical flame simulations.

The results show that the flame response follows the customary linear relationship as the limit $a \rightarrow 0$ is approached and the values given in Table 1 are different from those obtained in the case of steady-state flames and apply only for low to moderate rates of strain. Extended definitions that account for non-linear responses and further evaluation in the context of practical simulations of turbulent reacting flows is required. The inclusion of the above information into turbulent flow field calculations may be based on an approximation of the mean local rate of strain, which can be estimated on the basis of the integral time scale of turbulence. Here an efficiency factor, which is assumed to have the value of 0.28, has also been introduced.

NUMERICAL PROCEDURE

The present calculation method features consistent closures at the second moment level for velocity and scalar fields. The equations are discretised with a second order TVD scheme and the solution algorithm features a time-accurate, implicit generalized predictor-corrector method. The flows considered here include the planar duct configuration of De Zilwa et al (1999, 2000,2001) shown in Figure 2. The emphasis is on conditions producing strong combustion instabilities. It may, however, be pointed out that the transition from smooth to rough combustion at a constant Reynolds number is reproduced with reasonable accuracy. The transition process is influenced by impedances and wave propagation and boundary conditions (e.g. at the duct exit) are subject to significant uncertainties. Calculations with exit flow boundary conditions that provides approximately zero impedance as well as more complete simulations in which the computational domain has been extended significantly outside the duct have been performed.

Figure 2. Planar duct configuration of De Zilwa (1999, 2000, 2001).

The channel shown in Figure 2 is approximately two dimensional and the domain is resolved by two computational grids. The first is 1021x52 nodes and extends 300 mm upstream of the expansion plane to 680 mm downstream (corresponding to the duct exit). In the second grid, the duct is embedded in a domain that extends 800 mm beyond the duct exit and 75 mm (~ 2 exit duct heights) at the top and bottom of the duct. The total grid features 1280x102 nodes. The calculations consider fully compressible flow through the solution of the Reynolds averaged Navier-Stokes equations and transport equations for the reaction progress variable and the internal energy (Kuan et al 2002).

RESULTS

Computations of the configuration of De Zilwa et al (2001) for conditions giving raise to stable combustion have been performed along with the corresponding isothermal flow. The geometry comprises of a 160 mm wide rectangular duct of height 20 mm connected by a pair of 10 mm steps to another of the same width and 40 mm in height giving an expansion ratio of 2.0. This expansion ratio can be increased to 2.5 and 2.86 by increasing the step heights to 12 and 13 mm respectively with a pair of identical ramps. The duct extends downstream to a length of 680 mm. A compressor supplies air through a six-arm manifold into a 51 mm pipe, which is attached to the duct via a conversion section. Methane is introduced just downstream of the locations of air injection. The current configuration uses an expansion ratio of 2.86 with a Reynolds number of 20000 and bulk velocity of 22.2 m/s at the contraction exit.

For the conditions corresponding to stable experimental operation no significant unsteady features were found in the computations. Interestingly, however, the asymmetry in the non-reacting flow well reproduced in the computations as shown in Figure 3. Furthermore, the experimentally observed disappearance of this flow feature for the reacting flow was also found in the computations as indicated in Figure 4. The results shown for the isothermal and stably reacting duct flow are typical and can be viewed as encouraging.

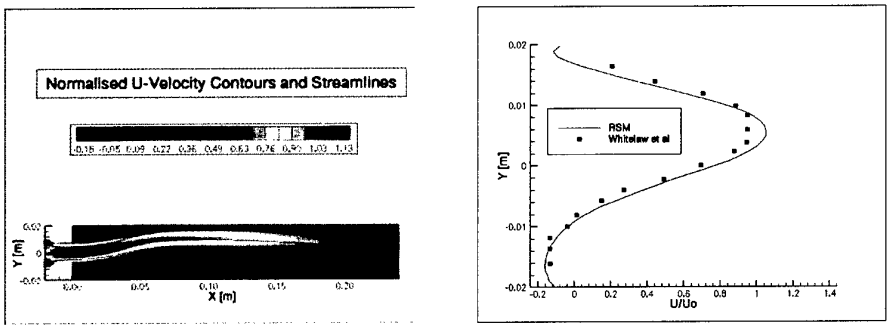

Figure 3. Example of comparisons of computational and experimental results for the isothermal duct flow of De Zilwa et al (2001). The computed results correspond to a second moment closure applied to the velocity field. The planar duct configuration features a contraction exit Re = 20000, U_o = 22.2 m/s, expansion ratio = 2.86 and step height (H) = 13 mm.

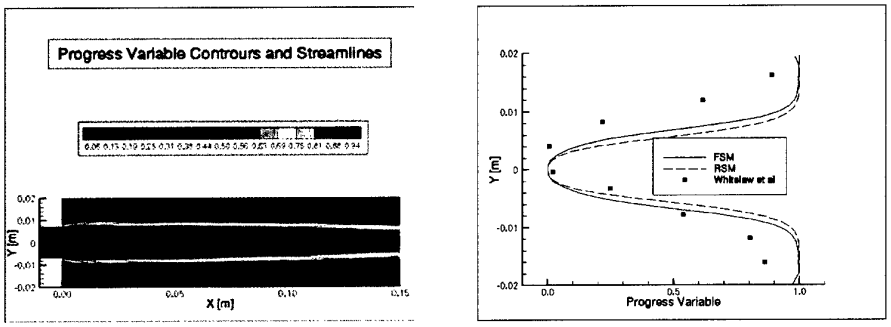

Figure 4. Example of comparisons of computational and experimental results for the reacting duct flow of De Zilwa et al (2001). The computed results correspond to a full second moment closure (FSM) and a second moment closure (RSM) applied to the velocity field only. The planar duct configuration features a contraction exit Re = 20000, U_o = 22.2 m/s, expansion ratio = 2.86 and step height (H) = 13 mm.

Calculations of the case corresponding to "rough" combustion are the main focus of the current work and much more demanding. The onset of instabilities as the stoichiometry is moved from 0.72 to 0.92 is well reproduced and evolution of the flow field for a full instability cycle is shown in Figure 5a. The calculation shown corresponds to approximately zero impedance at the duct exit and the periodic nature of the flow is evident and similar to that observed experimentally via CH fluorescence. The mean scalar fields, averaged across all phases, are shown in Figure 5b and correspond to the lower (25) and upper (26) limit reaction rate expressions discussed above. While the results would appear to

indicate that the latter expression is in closer agreement with experimental data, caution is required as the flame shape in the duct is strongly affected by the boundary condition at the duct exit.

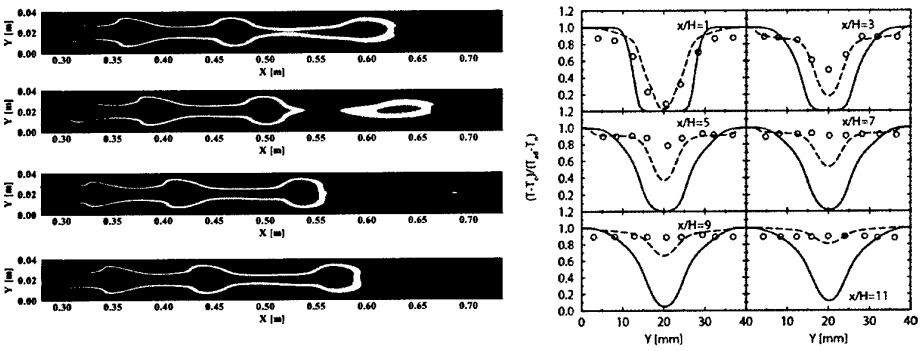

Figure 5. a. The evolution of the flow field illustrated via contour plots of the reaction progress variable corresponding to 0, 90, 180 and 270 degrees of the phase as measured by a pressure transducer 50 mm upstream of the expansion plane. **b.** Mean reaction progress variable profiles corresponding to the standard (solid line) and enhanced (dashed line) reaction rate closures.

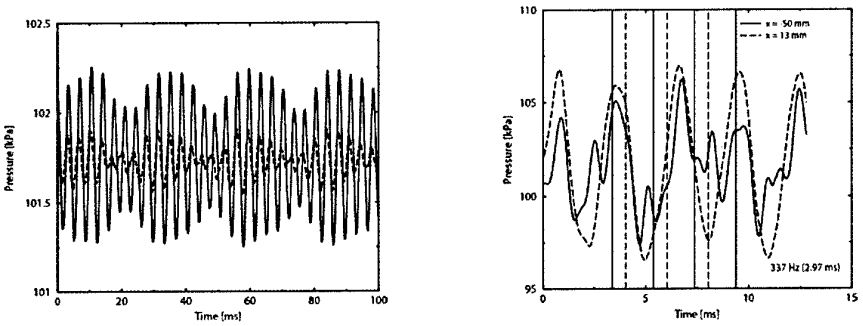

Figure 6. Pressure traces corresponding to the rough combustion case (ϕ = 0.92, u_l = 0.33 m/s, T_{ad} = 2148 K) of De Zilwa et al (1999,2000,2001) **a.** Standard reaction rate closure. **b.** Enhanced reaction rate closure. The 350, 110 and 230 degree phases are also indicated in the second figure and in both cases the solid line shows the pressure trace 50 mm upstream of the expansion plane and the dashed line downstream.

The pressure traces corresponding to the two reaction rate closures are given in Figure 6. The standard closure (Figure 6a) show two main modes with the dominant frequency around 288 Hz, which compares well with the 300 Hz recorded experimentally. There is also evidence of a lower mode around 40 Hz. The experimental and computed pressure amplitudes are 2 and 1 kPa and the lower limit expression thus results in an under-prediction. The upper limit expression (Figure 6b) leads to a corresponding over-prediction with a peak amplitude of 5 kPa and an increase in the dominant frequency to 337 Hz. The stronger excitation of the downstream oscillation and the appearance of an additional upstream mode is also evident. Comparisons of experimental and calculated results suggest that not all modes are well reproduced and that an improved treatment of impedances remains desirable. The axial bulk velocities obtained with the lower limit expression and corresponding to a 350 degree phase are shown in Figure 7a and the corresponding axial rms velocities in Figure 7b. In

the latter figure, the periodic and turbulence contributions are shown separately along with their sum. The agreement is similar for other phase angles. The calculations suggest that the periodic contribution to the rms fluctuations is important and that time-resolved measurements would be highly desirable. The complications arising with additional upstream modes and the possible interpretation of phase-averaged velocities for strongly reactive fuels are also evident. Despite the complexities inherent in the flows studied, the computational results illustrate that dominant frequencies are computed with good accuracy and pressure amplitudes are well within current uncertainties in the thermochemistry.

The calculations imply that the fluid mechanical aspects of the current combusting flows can be resolved by the computational technique and that the predominant uncertainties rest with the thermochemistry and the duct exit boundary conditions. The prevalence of local extinction and re-ignition cycles under fuel lean conditions further emphasizes the desirability of the inclusion of a more comprehensive treatment of interactions between turbulence and finite rate chemistry.

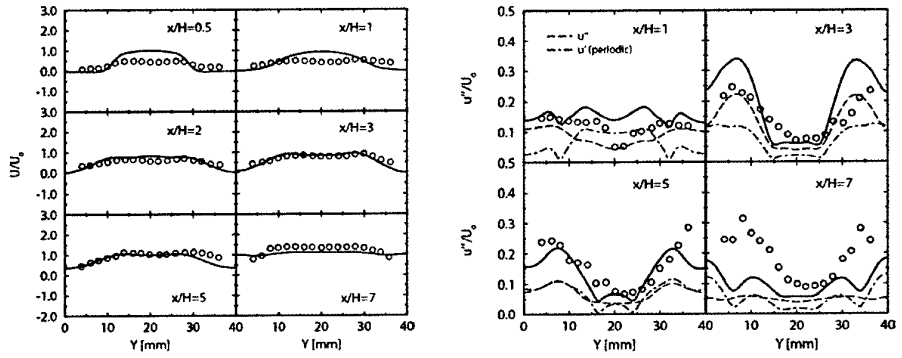

Figure 7. Axial mean and rms velocity profiles corresponding to a 350 degree phase for the case with rough combustion.

TREATMENT OF THE DUCT EXIT PLANE

The calculation discussed above show a notable absence of the second acoustic mode with a frequency of around 150 Hz. The implication is that the treatment of the duct exit flow boundary condition and the associated impedance is critical in the current geometry. The physical mechanism is intuitively clear and related to the density change encountered when the burnt gas exits the duct and mixes with ambient air. The temperature of the fluid mixture drops dramatically compared to the mixture immediately upstream of the duct exit. The existence of fluid mixtures of vastly different densities in the vicinity of the duct exit plane can be expected to strongly influence the nature of the pressure wave that is reflected back into the duct. The physics behind this process is difficult to capture using numerical boundary conditions and all attempts failed to yield reasonable results. Accordingly, the approach taken here is to extend the solution domain well outside the duct and thus to compute the full flow field corresponding to the jet mixing problem. Calculations show much more vigorous combustion downstream of the expansion plane due to reflected waves coming back into the domain. The complicated flow patterns at the duct exit are shown in Figure 8 and correspond to a calculation of the full second moment closure with the linear pressure redistribution model. In light of the complexity of the flow it may be readily appreciated that neither transmissive nor fully reflective conditions are appropriate.

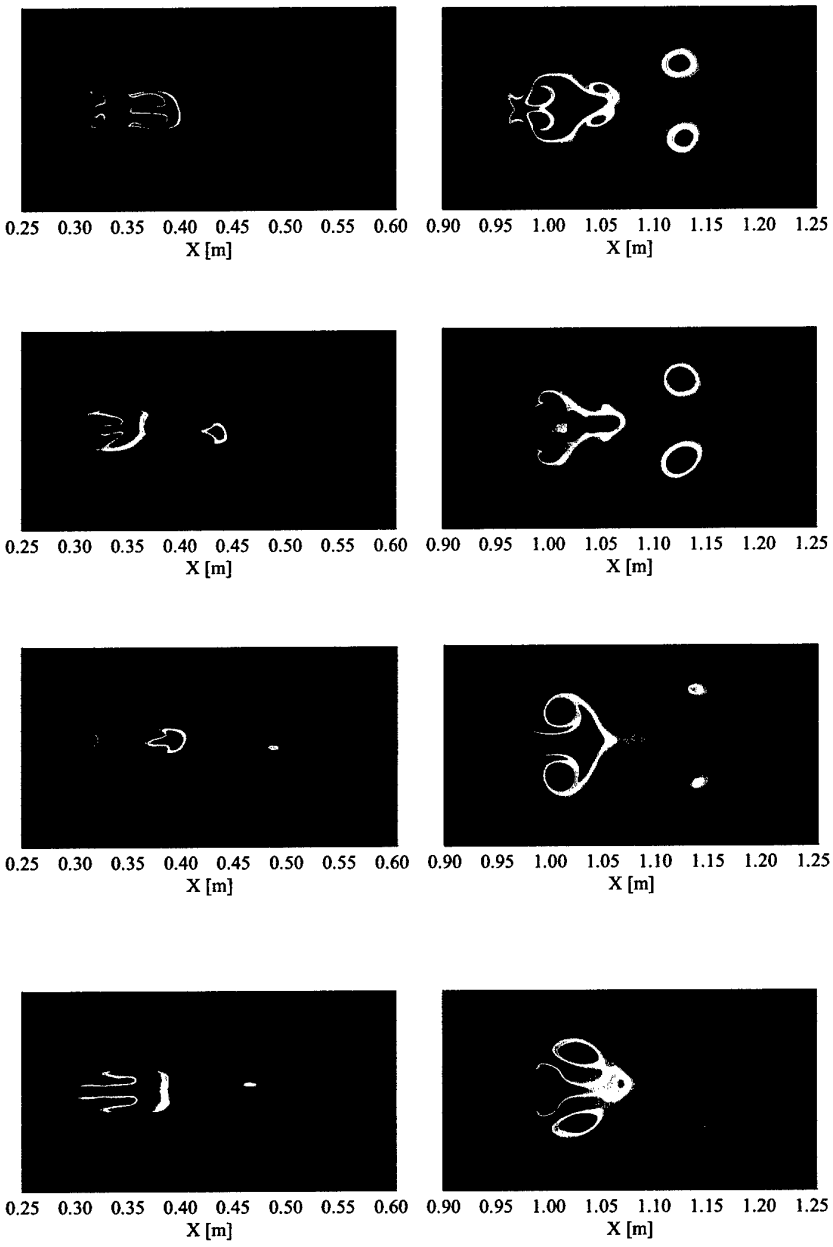

Figure 8. Flow pattern resulting from computations of the extended duct geometry including the flow outside the duct.

The further complications in the flow are readily apparent in the pressure trace shown in Figure 9a and an analysis of the latter reveals a dominant frequency at 225 Hz and, more importantly, additional modes at 101 Hz and 425 Hz. The peak pressure amplitude of ~ 5 kPa is higher than that recorded experimentally though it can be expected that further refinements in the treatment of the thermochemistry and flow at the duct exit will bring further improvements. It may also be noted that the agreement for the mean reaction progress variable as obtained with the standard reaction rate closure (25) is much improved as shown in Figure 9b.

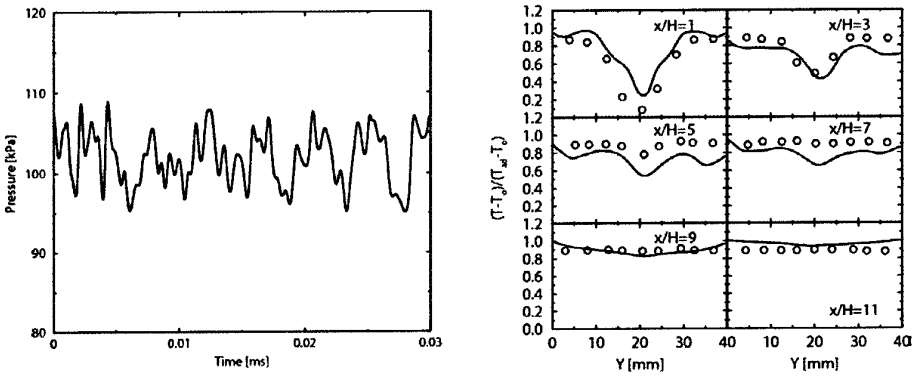

Figure 9. a. Pressure trace 50 mm upstream of the expansion plane as obtained with the computational domain extended beyond the duct exit plane. **b.** Mean progress variable profiles.

TIME-DEPENDENT HYBRID MONTE-CARLO AND FINITE VOLUME SIMULATIONS

The accurate modeling of extinction and re-light phenomena requires the introduction of direct chemistry effects in a manner that is combustion regime independent. The transported PDF approach uniquely offers the ability to deal with the key phenomena and the approach has the particular benefit that chemical reaction is treated in a closed form (i.e. as convection in scalar space) and that it may be applied in the context of different closure levels for the velocity field. The key advantage in the present context is the ability to include kinetically controlled/influenced phenomena, such as extinction and re-ignition. Such events play a key role in partially premixed systems operating close to the lean blow out limit. A further benefit is the ability to model the scalar spaces associated with diffusion, partially premixed and premixed systems within the same consistent framework. A concern in the practical application of such closures can be found in the balancing of computational resource and intrinsic scalar space requirements (e.g. Lindstedt 1998). To date transported PDF closures have only been applied in the context of steady flows and the current work extends hybrid Monte-Carlo/Finite Volume techniques to multidimensional time-dependent elliptic flows. In a further significant extension to past work the use of comprehensive systematically reduced chemistry is included.

Given the interest in the use of non-premixed combustion in the context of both flame stabilization techniques and current aero-engine technologies, computations have been preformed for bluff body stabilized flames at a range of Reynolds numbers. The equation set and solution technique outlined above has been augmented through the solution of a transport equation for the probability density function. For comparison purposes, a steady flamelet approach with mixture fraction and mixture fraction variance equations closed at the second moment level has also been used in order to further assess the accuracy of the flow-field predictions. The thermochemistry in the latter case is based on the traditional presumed beta PDF approach coupled with flamelets computed using comprehensive

detailed chemistry. By contrast, the transported PDF calculations features a large scalar space of 16 independent, 4 dependent and 28 steady state species and the chemistry applied is identical to that of the parabolic jet flame studied earlier by Lindstedt et al (2000). The same time-dependent elliptic calculation procedure applied above, featuring a second order accurate TVD scheme on a staggered grid, is used in the present context. The calculation is performed is a two-dimensional axi-symmetric geometry with a distributed 124x109 computational grid. Good temporal resolution is maintained with a Courant number not exceeding 0.1. Due to the need for comparisons with measurements, the fuel featured to date comprises of a mixture of natural gas and hydrogen. The flame under consideration here is the axi-symmetric bluff body stabilized diffusion flame investigated extensively over many years by Masri and co-workers (e.g. Dally et al 1998) at the University of Sydney. The burner geometry and layout is shown below.

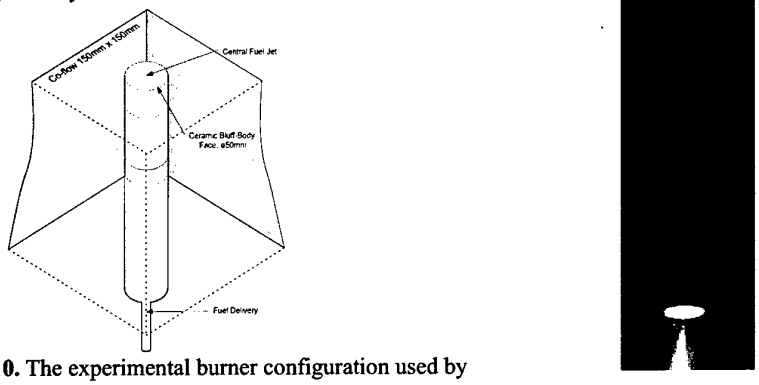

Figure 10. The experimental burner configuration used by Masri and co-workers.

The solution of the PDF transport equation (with a closure at the joint scalar level) is obtained using Lagrangian stochastic particles and the modified Curl's mixing model of Janicka et al (1979) is used. The computations have been performed on networked Intel Xeon 2.2 GHz dual processor Dell Precision 530 workstations using message Passing Interface (MPI) for inter-processor communication and the Scalable Parallel Random Number Generator (SPRNG) for generation of uncorrelated random number streams. Each available processor is assigned an equal number of particles and inter-processor communications required for the computation of the mixing process and compilation of global statistics. The speed-up is 1.94 and 3.84 over two and four processors and the parallel efficiency can be improved further by using a better network configuration. The fuel is CH_4/H_2 (1:1) and the jet velocity varies from 118 m/s (HM1E) to 214 m/s (HM3) with co-flows of 35 m/s and 40 m/s respectively and the flow instability observed experimentally in the upper shear layer is clearly reproduced as shown in Figure 11.

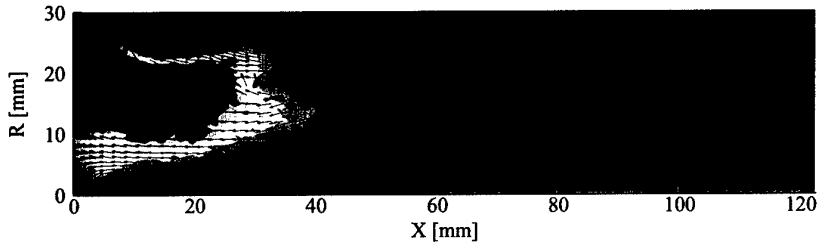

Figure 11. Instantaneous velocity field for the Sydney bluff body burner flame denoted HM1E obtained through the current unsteady RANS computation.

The agreement obtained for mean and turbulence velocities is very encouraging as shown in Figures 12 and 13 respectively. The same view may be held with respect to the shear stresses also shown in Figure 14. The resulting comparisons are averaged over O(10) instability cycles and the rms values shown in Figure 13 contains contributions from the periodic instabilities associated with vortex shedding. It would therefore appear that the current calculation method is capable of reproducing effects associated also with unsteady non-premixed combustion. The conclusion is given further support by the level of agreement obtained for the mixture fraction and the mixture fraction rms shown in Figure 15. The simple steady state flamelet approach used for the thermochemistry also results in reasonable agreement for temperature and species such as CO as shown in Figure 16.

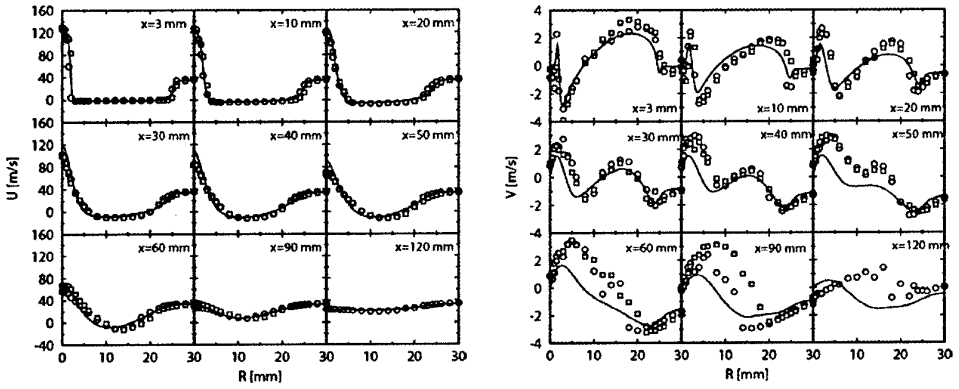

Figure 12. Mean velocity field for the Sydney bluff body burner flame denoted HM1E obtained through the current unsteady RANS computation.

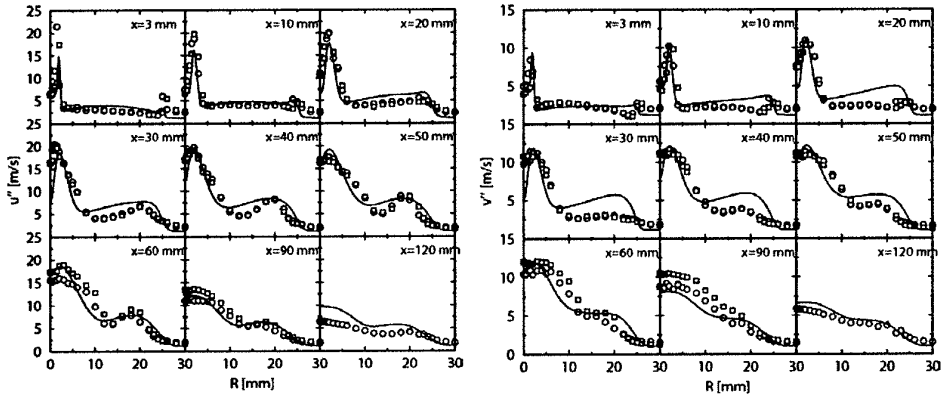

Figure 13. Turbulence fields for the Sydney bluff body burner flame denoted HM1E obtained through the current unsteady RANS computation.

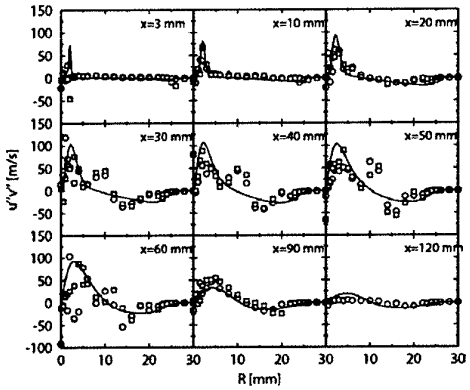

Figure 14. Shear stresses for the Sydney bluff body burner flame denoted HM1E obtained through the current unsteady RANS computation.

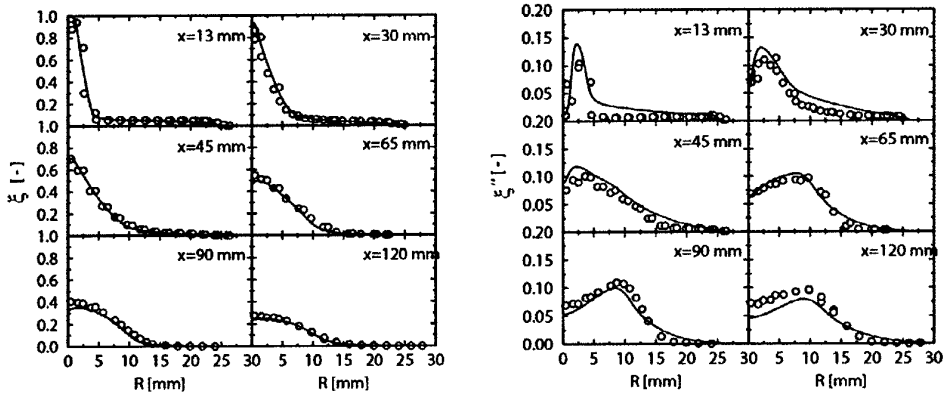

Figure 15. Mixture fraction and mixture fraction rms for the Sydney bluff body burner flame denoted HM1E obtained through the current unsteady RANS computation.

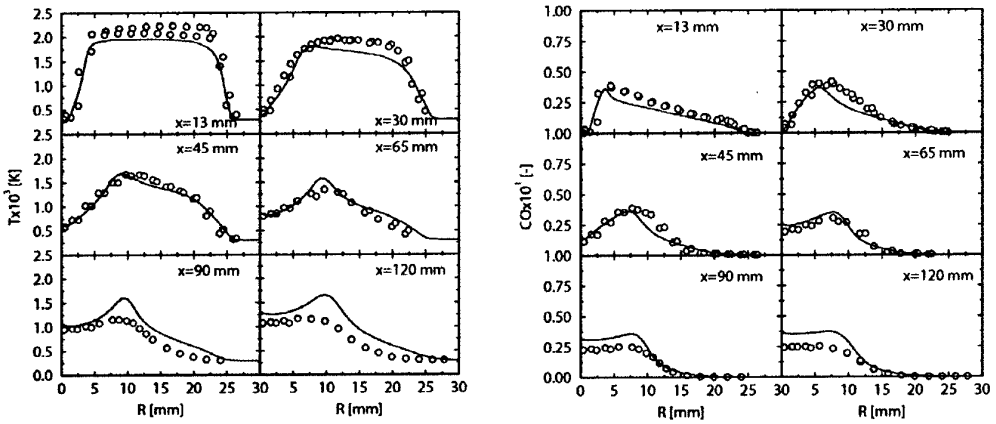

Figure 16. Scalar fields for the Sydney bluff body burner flame denoted HM1E obtained through the current unsteady RANS computation.

While the high Damköhler approximation used above is attractive due to the relative economy, more complete description of the scalar field is required to account for thermochemistry related effects. The corresponding transported PDF simulation is resolved with 120 stochastic moving particles per finite volume cell with the statistical properties evaluated using a "cloud-in-cell" type method (e.g. Birdsall and Fuss 1997). The computational domain is resolved using a 210x136 finite volume grid in an axi-symmetric geometry, extending from the bluff body surface to 250 mm in the axial direction and 100 mm in the radial direction. The velocity and scalar fields are initialized using the solution obtained based on the presumed beta PDF approach.

The thermochemistry is closed at the joint scalar level with the systematically reduced chemical reaction scheme for natural gas oxidation by Lindstedt and co-workers (e.g. Lindstedt et al 2000) The mechanism features 20 solved species, 28 steady state species and 300 chemical reactions. The velocity and turbulence fields serve as an input for the Monte Carlo solution while the scalar fields (e.g. species, temperature and density) are all evaluated from the joint probability density function. It is arguable that the mixture fraction and mixture fraction rms shown in Figure 17 are in excellent agreement with measurements. However, it is important to note that the simulation has only been averaged over one instability cycle and that startup effects are still present. The cooling effects of the startup vortex are clearly visible in the average profiles for species close to the bluff body as shown in Figures 18 and 19. However, the level of agreement obtained for nitric oxide (Figure 19b) is very encouraging – particularly as no adjustments to the thermochemistry used by Lindstedt et al (2000) have been made.

CONCLUSIONS

The controlling phenomena, observed experimentally and discussed in Part 2 of the current report, relate directly to the interactions of turbulence, chemistry and acoustics. The current work confirms the importance of all three components in determining confined combusting flows. The interactions must be modelled irrespective of the calculation approach used for the flow field and few previous studies have attempted to address them. However, Zhu et al (2000) showed that low frequency oscillations can be established through the interaction of unsteady combustion and boundary conditions and with frequencies consistent with those in aero engines. The application of the k-ε model was justified by the large separation in the frequencies of turbulent eddies and those of unstable bulk motion.

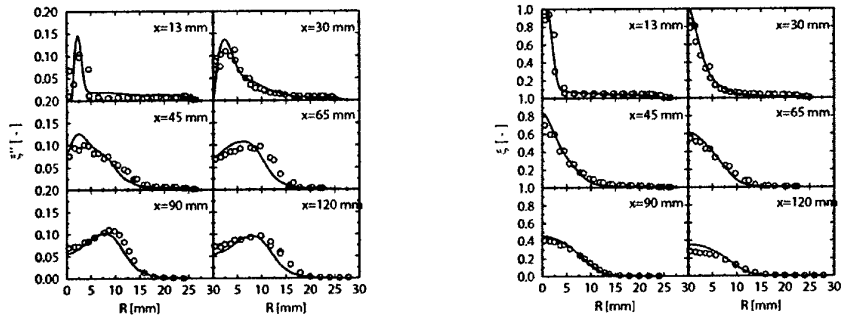

Figure 17. Mixture fraction and mixture fraction rms for the Sydney bluff body burner flame denoted HM3 obtained through the current hybrid unsteady RANS and stochastic Monte-Carlo simulation.

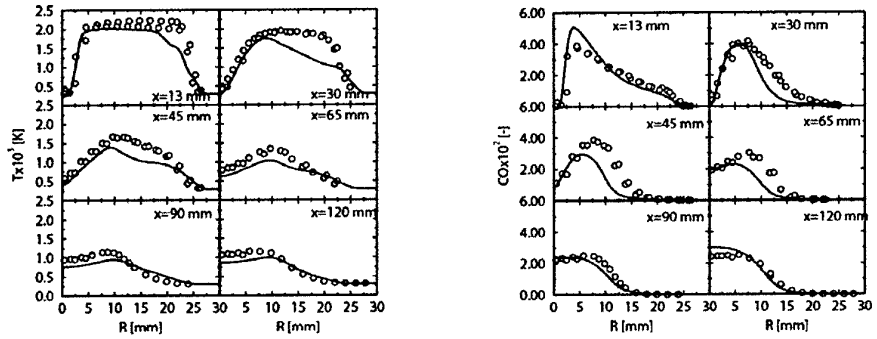

Figure 18. Extracted scalar fields for the Sydney bluff body burner flame denoted HM3 obtained through the current hybrid unsteady RANS and stochastic Monte-Carlo simulation.

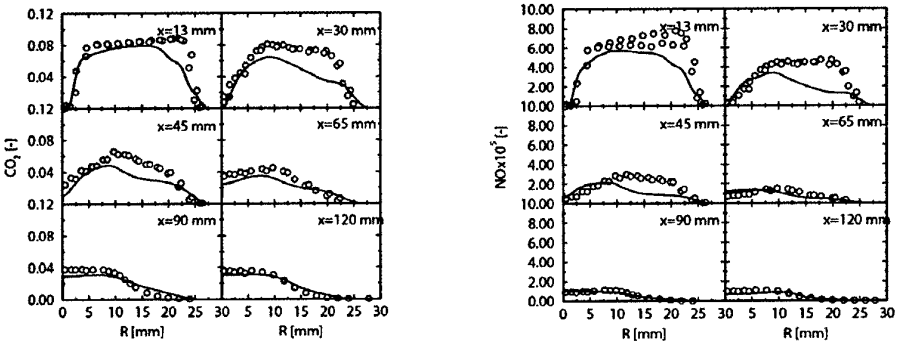

Figure 19. Extracted scalar fields for the Sydney bluff body burner flame denoted HM3 obtained through the current hybrid unsteady RANS and stochastic Monte-Carlo simulation.

Brookes et al (2001) applied a simple gradient based closure for scalar transport to model a bluff body stabilized premixed flame and showed that the transition from rough to smooth combustion could be reproduced. None of these studies considered detailed comparisons with measurements and the use of gradient transport approximations, arguably justifiable in non-premixed combustion, is not appropriate with partially premixed or premixed combustion where non-gradient transport may be induced by pressure gradients. Indeed, the use of second moment closure applied exclusively to the velocity field is also unsatisfactory (Lindstedt and Vaos 1998). The complexities associated with the current flows are formidable and the qualitative and quantitative levels of agreement obtained are very encouraging. The current work also shows that time-dependent hybrid stochastic and finite volume methods can be successfully applied in conjunction with large scalar spaces and thus enable accurate computational studies of extinction-relight phenomena in lean burn combustion devices.

PART 2: EXPERIMENTS

Tasks, 2, 5, 7 and 8 of the Proposal required that experiments be performed in support of the calculations, and specific items were noted including the examination of the preferred location of injection of fuel to assist stabilization and the possible benefits of unsteady injection. The experiments described by Emiris and Whitelaw (2002, 2003) go some way to fulfilling these obligations and those described below complement them and fulfill the objective while leaving unknowns to be addressed by future research. The new experiments and results are presented in the context of those of Emiris and Whitelaw so that only a small number need be repeated here.

This second part of this final report has been prepared in four sections dealing respectively with the flow arrangements and instrumentation, visualization, flammability and stability, and the effects of wall temperature, some aspects of control, co-axial flows and non-premixedness and conclusions. The following section is brief since most of the information has been documented previously and the penultimate section is also short since the research was begun in late 2002 as an early examination of a topic intended for later and more thorough research.

FLOW ARRANGEMENT AND INSTRUMENTATION

Experiments performed with methane, ethylene and propane fuels, premixed with air, continue and include the determination of flammability and stability limits and the effects of duct wall temperature on them, the nature of combustion instabilities and aspects of control. The arrangement was similar to that used by Emiris and Whitelaw (2002, 2003) and comprised, figure 20, an upstream duct 51 mm in diameter and 1030 mm long and a downstream duct of 80 mm in diameter and 1030 mm long. Part of the downstream duct was replaceable with a modified section including a quartz window to allow visualisation of the step region. A swirl register, in which the gases were premixed, had an acoustic impedance of unity and closed the upstream end while a screen and a length of honeycomb subsequently removed the swirl and ensured well-mixed two-dimensionality of the flow at the expansion plane. The increase in diameter provided a sudden expansion on which the flames stabilised and the downstream end was open.

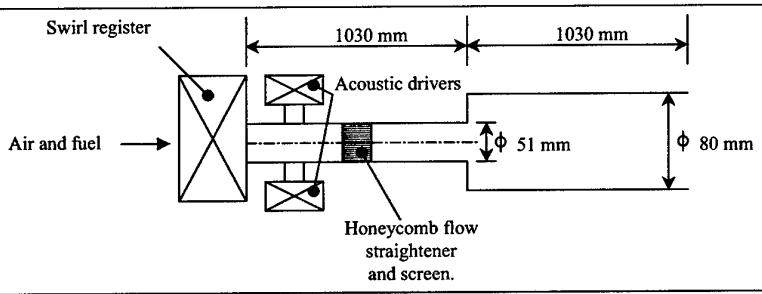

Figure 20: Round sudden-expansion configuration with acoustically closed upstream end and facility for oscillating pressure field. Not to scale. All dimensions in mm.

The flow rates were regulated to a precision of 3% by calibrated float-rotameters (Rotameter Manufacturing Co. and KDG Instruments) and the mass-flow rates through the combustor are presented in terms of the Reynolds number based on the bulk velocity and duct diameter of the upstream duct. Extinction was determined by observation and photographic visualisation presented in true colour (Kodak Digital Science DC210 Zoom Camera), while a Pt-Pt/13%Rh thermocouple with 200 μm diameter wires determined the wall temperature from 10 cm upstream of the expansion plane to 100 cm downstream and, since spectra showed the response time of the thermocouple was about 500 Hz, temperature data was collected at a rate of 1 kHz and over a period of 4 s to provide a mean value.

Further instrumentation included a water-cooled piezo-electric transducer (Kistler 6121 and charge amplifier 5007) mounted flush with the pipe wall 70mm upstream of the expansion plane with the signal fed through an interface (National Instruments DAQ BNC-2090 and PCI MIO 16E4 A/D card) to a computer for acquisition (LabView software) of 8 seconds of data per condition at a sampling rate of 4096 Hz. The active feed back system comprised a band-pass filter (Krohn-Hite Model 3202) with a custom-built phase locked loop to produce an output signal that was frequency and phase-locked to the dominant mode of the duct (typically around 160 to 180 Hz) and fed back with variable phase-delay through a custom built stereo amplifier (51 W) to acoustic drivers that caused destructive or constructive interference. Post-processing of the pressure signal involved custom written software (Metrowerks C++) and implementation of a recursive Fourier analysis algorithm using the Hanning function with each data interval of 1 s and 50 % overlap to give a resolution of 1 Hz.

Table 2 lists the lower heating value and adiabatic flame temperatures at stoichiometric conditions and standard ambient temperature and pressure, taken from Turns (2000) and, laminar flame speeds at the equivalence ratio of 0.7 from Egolfopoulos et al. (1990) for the three fuels.

	Lower Heating Value (kJ/mol)	Adiabatic Flame Temperature (K)	Laminar Flame Speed (m/s)
Methane, CH_4	800	2226	0.20
Ethylene, C_2H_4	1321	2369	0.36
Propane, C_3H_8	2040	2267	0.24

Table 2: Thermochemical constants for mixtures of air and methane, propane and ethylene. Adiabatic flame temperature is at $\phi = 1.0$ and standard temperature and pressure. Flame speeds are at $\phi = 0.7$.

The table indicates that combustion of methane generates the smallest amount of energy per molecule and because it comprises the fewest carbon and hydrogen atoms while propane releases the most heat per molecule. The quantity of oxygen available for combustion in a given volume of air is

fixed, however, so that fewer molecules of propane can be burnt per unit volume of a stoichiometric mixture. Thus, the balance between energy released per molecule and the number of molecules burnt per unit volume means that the adiabatic flame temperatures of methane and propane are within 5 %, and that of ethylene is greater by about 100 K. Ethylene also has the fastest reaction rate and methane the slowest, as is evident from the laminar flame speeds in the table.

VISUALISATION

A quartz widow was used to observe the step and photographs presented in Figure 21 show the mean luminosity and its distribution for lean methane- and ethylene-air flames at identical conditions, chosen to highlight the difference between the two fuels. It is evident that methane-air flames stabilised approximately 4 step-heights downstream of the expansion while ethylene flames were in contact with the step and partially distributed upstream along the expansion plane. Similar observations with propane showed that, as with methane, stabilisation occurred downstream of the expansion with no distribution of heat-release upstream.

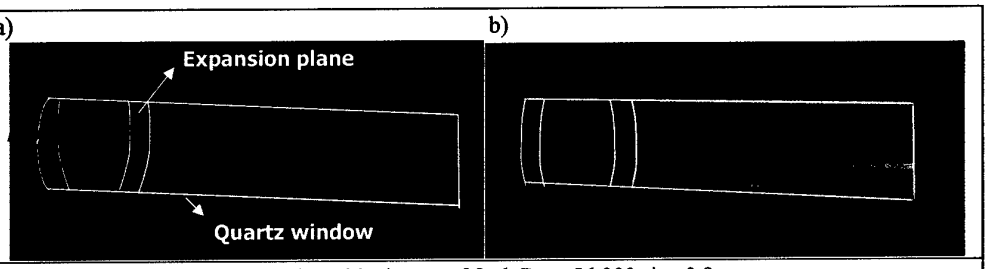

Figure 21: Mean flame luminosity with change of fuel. Re = 56,000, $\phi = 0.9$,
a) Methane-air, b) Ethylene-air

The photographs also show that ethylene flames were more luminous and this was expected from the greater density of CH radicals produced during combustion, while the red glow evident in the ethylene photograph was due to the higher flame temperature and speed that led to greater heating near the step region of the steel duct.

FLAMMABILITY AND STABILITY, AND THE EFFECTS OF WALL TEMPERATURE.

A typical profile of mean temperature along the duct wall at equilibrium is given in Figure 22, which shows a sharp increase from a minimum of less than 300 K at 10 cm upstream of the expansion, to a maximum of 950 K 34 cm downstream, after which there was a gradual decline towards the open end of the duct. The maximum in temperature downstream of the expansion was expected from the photographs, which showed that the flame stabilised in this region and the sharp drop in temperature further upstream was a consequence of heat loss to the oncoming cold reactants. The products were hot and the rate of cooling was much slower downstream of the temperature peak.

The flame temperature varied with equivalence ratio and this was reflected in the peak temperature at equilibrium, which was almost 1000 K with near-stoichiometric mixtures, but less than 700 K near the lean extinction limit. The temperature distribution was uniform at around 300 K at start-up conditions and increased with time until equilibrium was established after about 10 minutes.

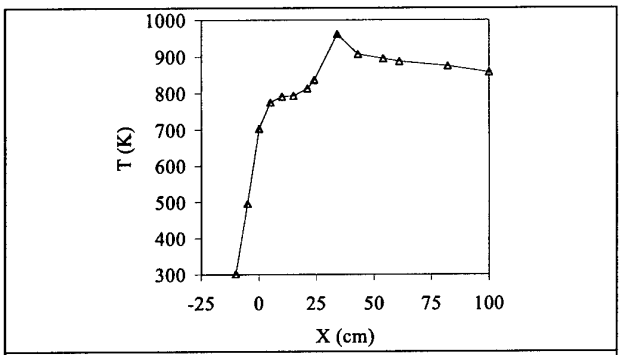

Figure 22: Profile of wall temperature at thermal equilibrium, Methane-air , Re = 39,500, ϕ = 0.89, X = distance downstream of the expansion.

The flame extinguished at equivalence ratios that depended on the maximum wall temperature, as shown in Figure 23 for mixtures of air and methane and ethylene. The burner was operated at stoichiometric conditions until the desired temperature was reached, after which the fuel flow rate was reduced quickly and the temperature at extinction noted. Sample measurements with propane-air mixtures showed results slightly to the left of those with methane and with similar curvature.

The figure shows that the lean limit at a Reynolds number of 39,500 varied from equivalence ratios of 0.64 to 0.5 with methane and wall temperatures from 400 to 900 K respectively and from 0.48 to 0.33 with ethylene and the same increase in temperature. At any given temperature, the lean extinction limits were smallest with ethylene and largest with methane and this is qualitatively comparable to the faster flame speeds of ethylene in Table 1. The change in the equivalence ratio of lean extinction with increase in temperature is not surprising since flame speed decreases with equivalence ratio and increases with temperature and it is likely that partial pre-heating was responsible for the increasingly lean extinction limits. It is also evident that lean extinction occurred in ethylene at the equivalence ratio of 0.48 and cold operating conditions while methane extinguished at the same equivalence ratio under hot operating conditions. It should also be noted that, regardless of temperature, extinction did not occur above a critical equivalence ratio, 0.48 with ethylene and 0.65

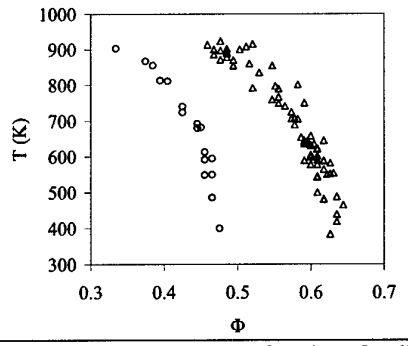

Figure 23: Lean flammability limits as a function of wall temperature. Re = 39,500, circles are ethylene and triangles are methane.

with methane. Similarly, provided the equivalence ratio is not zero, extinction is not expected to occur above a critical temperature and this is consistent with the curvature of data in Figure 23 and with the limit temperature of 1200 K suggested by Law et al. (1986) for lean hydrocarbon flames.

The process of extinction at any point of the curves of Figure 23 was similar with low frequency amplitude modulations of the dominant mode and increasingly high peak-to-peak values as it was approached, particularly at high Reynolds numbers and with low wall temperatures where a large modulation was often followed immediately by extinction. De Zilwa et al (2001) observed the same phenomenon with methane and hot operation showed peak amplitudes of the order of 1 kPa immediately prior to extinction, as shown in Figure 24 in a round duct without constriction.

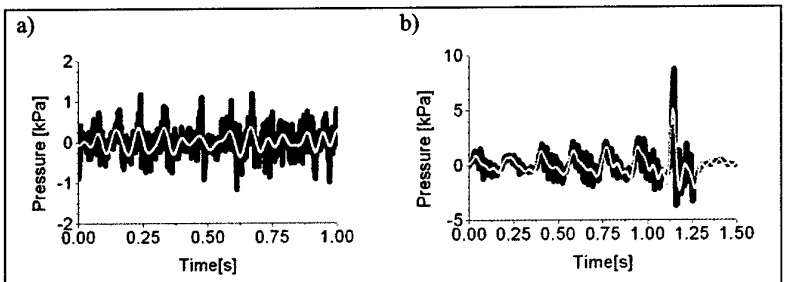

Figure 24: Pressure signals at extinction with methane-air mixtures. A) Re = 68,000, unconstricted duct, b) Re = 35,000, constricted duct. Black: Unprocessed signal. Light grey: Processed to show modulations.

It is also evident that the peak amplitudes of the modulation and acoustic pressure signals were up to 5 and 10 kPa respectively with an exit nozzle, occurred immediately prior to extinction and due to coupling between the cyclical extinction-and-relight and a bulk mode oscillation at around 35 to 50 Hz. In the present experiments with an open downstream end and three fuels, there were similar modulations in amplitude close to extinction and Figure 25 shows an explosive modulation of peak amplitude around 10 kPa in the pressure trace of an ethylene-air flame after 4 seconds of data collection and lasting 200 ms, after which it extinguished. In this case, there was an increase in the peak amplitude of the upstream ¼ wave (at around 80 Hz) from 2 to 4 kPa over 50 ms after which there was a sharp transition to the ¾ wave of the entire duct (175 Hz) so that the coupling was between two acoustic frequencies rather between acoustic and an extinction-and-relight frequencies.

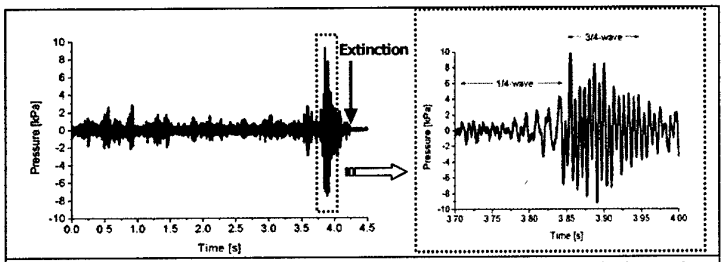

Figure 25: Instantaneous pressure signal at extinction of an ethylene-air flame in the unconstricted duct.
Re = 76,000, ϕ = 0.69

The change in the dominant frequency in near-limit ethylene flames contrasts with that of methane or propane where it remained constant and was modulated by extinction-and-relight. The different behaviour may be explained by the higher speed of ethylene flames, and the photographs of Figure 21 show that they stabilised close to the step with a propensity to flash upstream, while methane or propane-air mixtures stabilised further downstream and did not influence the upstream region. Extinction did not occur with higher equivalence ratios but the region of stable low-amplitude combustion ended at the lean stability limit, where a small increase in equivalence ratio led to a large increase in the rms of pressure fluctuations. Figure 26 shows that the locus of the region of instability was dependent on the fuel type and occurred at increasing equivalence ratios with ethylene, propane and methane, namely 0.68, 0.82 and 0.85 respectively at the Reynolds number of 39,500 corresponding to energy release rates of 150, 167 and 170 kW.

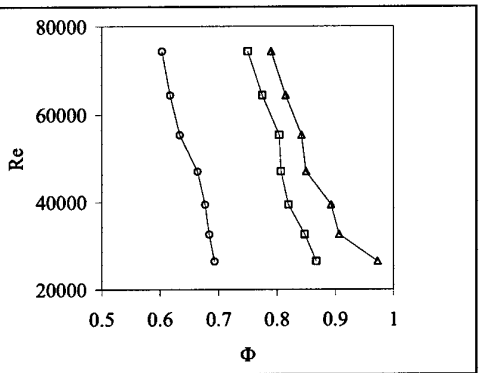

Figure 26. Lean stability limits for methane (Triangles), Propane (Squares) and Ethylene (Circles)

Transition to unstable combustion occurred above similar rates of heat release, to within 12 % for the three fuels, and suggests that the origin of the instability was a consequence of Rayleigh amplification of acoustic waves. The stability limits were unaffected by wall temperature so that they were probably unrelated to extinction and indicating that it was not the heat-release rate that led to the transition to unstable combustion. Since an increase in Reynolds number increased the rate of combustion, the effect was to increase the range of equivalence ratios at which high amplitude oscillations were observed. Lindstedt et al. (2003) has also reported the relationship between stability limits and heat-release rate.

Figure 27 shows the flammability and stability limits for methane and ethylene together with profiles of the normalised rms of pressure fluctuations. As discussed previously, very lean mixtures led to extinction while large-amplitude oscillations occurred with intermediate values and, with excessively rich mixtures, the methane flame at the step blew off to form a partially premixed flame stabilised at the open end of the duct. At Reynolds numbers greater than 60,000, the methane partially premixed flame led to excitation of the full-wave frequency of the entire duct and amplitudes well in excess of 10 kPa. The rich flammability limit shown for ethylene corresponds to the equivalence ratio at which the flame blew off at the step, and acoustic generation from the downstream flame occurred at Reynolds numbers of around 50,000. Thus, the rich flammability limit was difficult to quantify and the results of Figure 27 should be regarded as approximate.

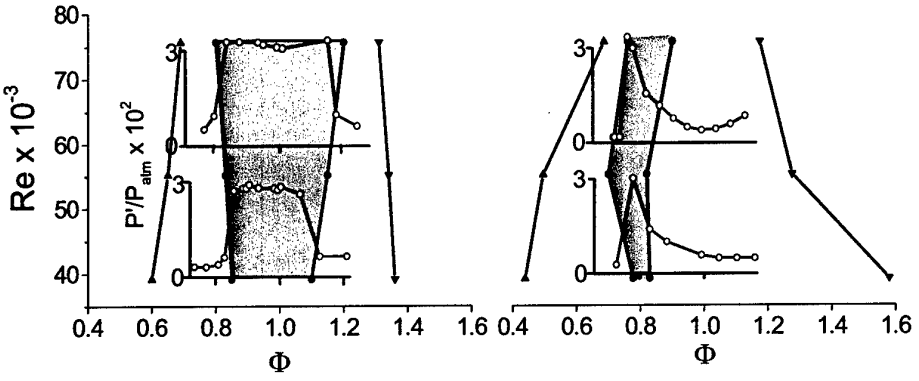

Figure 27: Flammability and stability limits a) methane-air, b) ethylene-air ▲ – Lean limit, ▼ – Rich limit, unstable region is shaded. o – Rms pressure amplitudes superimposed for Re = 39,500 and 55,400

The high-amplitude rms pressure fluctuations for methane were near symmetric about stoichiometry at the two Reynolds numbers shown and for interim values. In contrast, ethylene gave rise to a maximum close to an equivalence ratio of 0.8 and a minimum at stoichiometry, after which a steady increase was again apparent towards the rich flammability limit as a consequence of the strengthening partially premixed flame at the duct exit, particularly at high Reynolds numbers. The reason for the minimum in amplitude close to stoichiometry for the ethylene flames is explained by the corresponding spectra of the pressure fluctuations, Figure 28, that indicate the co-existence of dominant frequencies based on the upstream and overall lengths of the duct. The excitation of upstream modes was expected from the photographs that showed ethylene flames stabilised close to the expansion step so that even relatively small oscillations were sufficient to move the flame upstream.

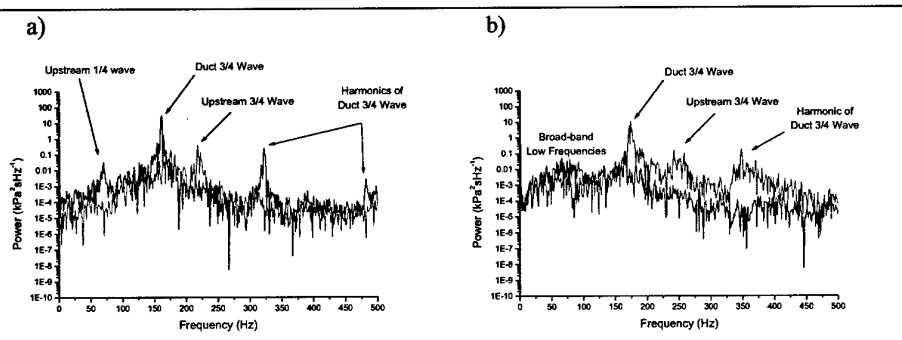

Figure 28: Power spectra of pressure fluctuations. Ethylene: red line. Methane: black line. a) Re = 60,000, ϕ = 1.0, b) Re = 74000, ϕ = 0.7

Thus, the spectra for ethylene and methane flames at stoichiometry had a peak at around 165 Hz corresponding to the dominant ¾ wave of the entire duct, and that for ethylene had an additional peak at 220 Hz corresponding to the upstream ¾ wave. The boundary conditions for the upstream ¾ wave and that of the entire duct are incompatible, the former requiring a pressure node at the

expansion plane and the latter a pressure antinode, so that the competing upstream frequency limited amplitudes with ethylene. The tendency for ethylene to flash back, and the subsequent excitation of resonant modes associated with the upstream duct, was also observed in preliminary calculations of Lindstedt et al. (2003).

Other features of the spectra at stoichiometry include the excitation of higher harmonics and a small peak at around 60 Hz suggesting weak excitation of the lower ¼ wave harmonic. The figure also suggests that the dominant frequency for ethylene was slightly higher than that of methane, by about 8 Hz, and this is likely to be a consequence of the higher flame temperature of ethylene that shortened the acoustic length of the duct. Spectra for propane-air flames at stoichiometry were similar to those of methane and did not show any evidence of flash back upstream of the expansion.

Spectra of pressure fluctuations at the leaner equivalence ratio of 0.7 and in the region of near-stable combustion bounded by the flammability and stability limits, Figure 28b, show a broad-band peak at frequencies less than 100 Hz, associated with extinction and relight and less obvious at stoichiometry particularly with ethylene. The overall amplitudes were smaller and, since this reduced the extent to which the ethylene flame could be translated upstream of the step, the upstream ¾ wave frequency was weakened while harmonics of the ¾ wave of the entire duct strengthened. Propane flames, as with methane, showed a general reduction in the amplitude of all frequencies above 100 Hz, and an increase below due to extinction and relight.

SOME ASPECTS OF CONTROL

Attempts to control the oscillations involved the addition of small quantities of fuel in the region of highest strain-rate at the sudden expansion so as to improve resistance to extinction with subsequent stabilisation, and passive and active control with oscillations imposed by acoustic drivers. The passive acoustic control experiments made use of harmonics of the duct while active control involved a phase-locked loop to determine the natural phase of oscillation and a shifter to change it by a value chosen according to flow conditions after which the control signal was fed back into the duct through the acoustic drivers. Pressure signals of Emiris and Whitelaw (2003) are shown in Figure 29 when the methane-air mixture was at an equivalence ratio of unity and passive forcing and added fuel each contributed to reductions in amplitude.

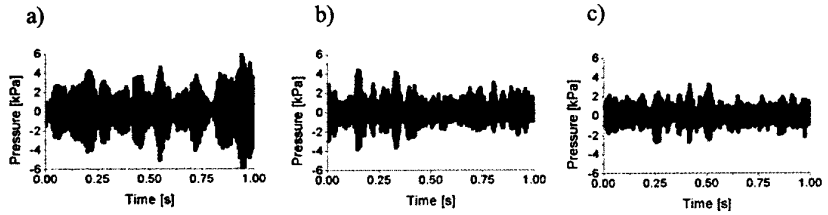

Figure 29: Effect of forcing and fuel injection on the time-resolved pressure signals, Re= 71,000 and $\phi = 1.0$. Unconstricted duct.
a) Naturally-occurring flow, b) forcing at 380 Hz and input power of 51 W and c) 3%-added fuel and forcing at 380 Hz and input power of 51 W.

The measurements of Figure 30 show the sensitivity to fuel injection rate near the lean extinction limit at the equivalence ratio of 0.6 and the relatively low Reynolds number of 26,501. It is apparent that 1.9 % fuel injection had almost no effect while a 65 % reduction in amplitude, from 0.079 to 0.051 kPa, was observed with 3.8 % injection. Further increase to 5 % added fuel destabilised the flame so that the amplitude was 32 % greater than that of the natural flow, at 0.104 kPa. It is clear that there was a very narrow range of operation in which fuel injection had a positive effect on stability. This is to be expected since injected fuel was diluted by the oncoming lean flow and small

quantities would have negligible effect at the expansion plane while excessive quantities of fuel would reduce the degree of premixedness at the step and hence reduce the resistance to strain so that a destabilising effect was observed. The position of the injectors is important, as noted by Emiris and

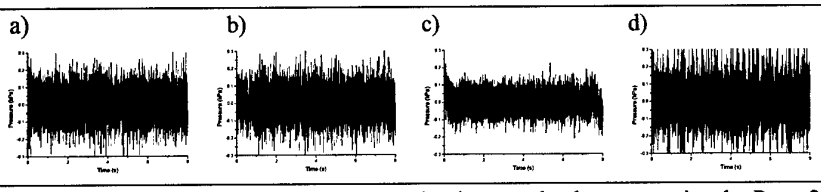

Figure 30: Effect of fuel injection rate on the time-resolved pressure signals, Re = 26,501, ϕ = 0.6. Unconstricted duct.
a) Naturally occurring flow, b) 1.9 % added fuel, c) 3.8% added fuel, d) 5 % added fuel.

Whitelaw (2003), and the optimum is likely to vary with Reynolds number and fuel injection rate. Emiris (2002) considered the equivalence ratio of the injected mixture and pure fuel was reported as most effective at the Reynolds number of 60,000 and at an over-all equivalence ratio of 0.63, but extension of these results to a wider range of operating conditions is desirable.

It is evident that the addition of small quantities of fuel can have beneficial effects but within limited ranges that depend on equivalence ratio, Reynolds number and gas and experiments are continuing to explain the different observations. The stabilising effects of added fuel have been shown to be less necessary with the faster flame speed of ethylene, as evident in the lower levels of low frequency noise in the spectra of Figure 28, but extinction and relight remains, together with its modulation effects, and acoustic oscillations can transport injected fuel away from regions that are critical for stability and also increase instantaneous strain rates with increased need for improved stabiliation.

Passive and active control with imposed acoustic oscillations were successful in reducing the amplitude of methane-air mixtures, as shown in Figure 31, where it is apparent that oscillations

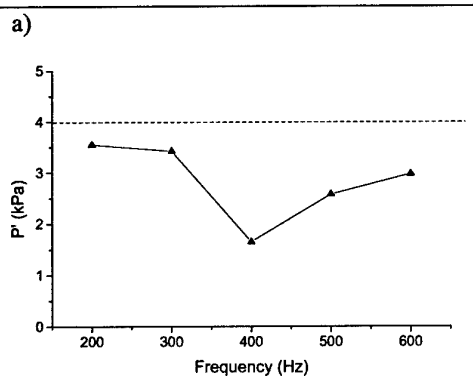

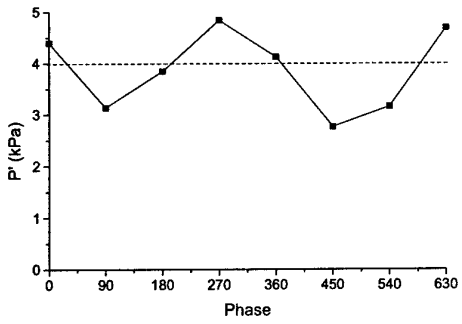

Figure 31: The rms of pressure fluctuations with methane-air mixture, Re = 55,400, $\phi = 0.8$
Dashed line: amplitude of naturally occurring flow, (All oscillations imposed at 51 W)
a) Passive control, rms as a function of frequency of imposed oscillations
b) Active control, rms as a function of phase shift.

imposed at a frequency of 400 Hz, close to the second harmonic of the duct ¾ wave, led to the greatest reduction in amplitude, from 4 to just under 2 kPa. It should also be noted that oscillations imposed at 200 Hz, corresponding to the first harmonic of the ¾ wave, had the smallest effect. With active control, the frequency was that of the first harmonic due to its greater amplitude and ease with which the loop could lock on to the signal. The greatest reduction in amplitude, from 4 to 3 kPa, occurred with a 90-degree phase shift, while passive control could only provide a reduction to 3.5 kPa at the same frequency. Constructive interference was evident at 270 degrees, leading to an increase in amplitude from 4 to 5 kPa, and the pattern was again repeated, as the phase was shifted further at 90-degree intervals to 630 degrees. The cyclic relationship between phase and oscillation amplitude was expected as a consequence of interference and shows that the acoustic drivers imposed a pressure oscillation amplitude of 1 kPa at the expansion plane. The natural oscillations had an amplitude of 4 kPa so that drivers of greater power are likely to provide better control. Active control provided greater benefits than passive control at 200 Hz and even greater benefits may occur with the phase locked to other harmonics of the natural oscillation frequency, such as that at 400 Hz. It also remains to be determined whether or not the same approach will yield similar results with ethylene and to quantify the effects of modulation amplitude on control.

CO-AXIAL FLOWS AND NON-PREMIXEDNESS

The possibility of extending the experiments to include non-premixed fuel and air has also been examined with preliminary experiments in the configuration of Figure 32. This coaxial arrangement was used to provide an annulus to core area ratio of unity with equal flow-rates, to minimise shear and to preserve non-premixedness. Early results showed that the flammability limits were a function mainly of the annular equivalence ratio, with near-stoichiometric mixtures providing the broadest range of operation, while the range of stability was reduced with increasing equivalence ratio in the central core.

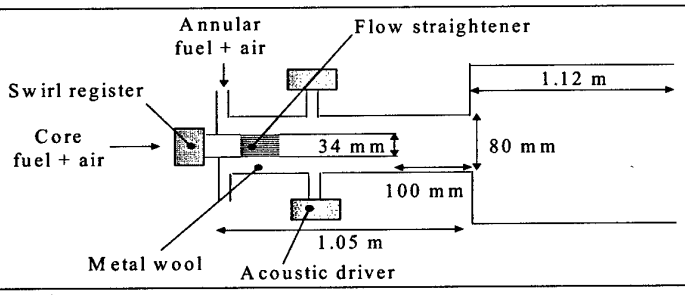

Figure 32: Coaxial duct arrangement.

CONCLUDING REMARKS

Ethylene-air mixtures had the highest flame speed for any given equivalence ratio while methane had the slowest and this was reflected in the wider flammability and stability limits of ethylene relative to methane and propane, which had similar limits and flame speeds. Increase in the downstream wall temperature to a maximum of almost 1000 K, allowed partial pre-heat of the mixture as it flowed past the step, increasing the flame speed and widening the flammability limits. The stability limits were not a function of downstream wall temperature, even though mixtures with higher flame speeds led to wider instability, and this confirms that the amplitude of oscillations increased only with heat-release rate.

The faster flame speed of ethylene had the further consequence that the flame moved upstream of the step and subsequent excitation of acoustic modes associated with the upstream duct, particularly the ¾ wave near stoichiometry, meant that a natural control mechanism prevented large overall amplitudes. Upstream movement of the flame was not observed with methane of propane and spectra showed further that the amplitude of low frequencies associated with extinction and relight was lowest with ethylene, as expected from its greater resistance to strain.

Passive control with fuel injection was demonstrated at lean and stoichiometric conditions, but within narrow intervals of operation for each condition and further research is required to optimize important parameters such as injector to step separation, injection flow rate and injector mixture equivalence ratio for a range of Reynolds numbers and equivalence ratios. Passive acoustic control was also demonstrated over a range of frequencies and proved most effective at the second harmonic of the duct ¾ wave, at 400 Hz, while active control produced better results at 200 Hz and even greater improvements are likely with 400 Hz.

ACKNOWEDGEMENTS

This research was carried out with financial support from the United States Army under Contract N68171-00-C-9019. Useful discussions, advice and practical assistance with and from Drs. S Fletcher, H McDonald, A M Marquis, S Sampath and S Sivasegaram are gratefully acknowledged. The indispensable contributions of Mr T S Kuan, Dr E M Vaos, Dr I Emiris and Dr E Korusoy are also gratefully acknowledged.

REFERENCES

Birdsall C K and Fuss D (1997) Clouds-in-Clouds, Clouds-in-Cells Physics for Many-Body Plasma Simulations, J. of Comp. Phys., **135**, 141-148.

Bray K N C, Champion M and Libby P A (2001) Pre-mixed Flames in Stagnating Turbulence: Part V – Evaluation of Models for the Chemical Source Term, Combust. and Flame, **127**, 2023-2040.

Brookes S J, Cant R S, Dupere I D J and Dowling A P (2001) Computational Modeling of Self-Excited Combustion Instabilities, Transactions of the ASME, **123,** 322-326.

Dally B B, Masri A R, Barlow R S and Fiechtner G J (1998) Instantaneous and Mean Compositional Structure of Bluff-Body Stabilized Nonpremixed Flames. Combust. and Flame, **14**, 119-148.

De Zilwa S R N, Emiris I, Uhm J H and Whitelaw J H (2001) Combustion of Premixed Methane and Air in Ducts, Proc. R. Soc. Lond. A, **457**, 1915-1949.

De Zilwa S R N, Sivasegaram S and Whitelaw J H (1999) Control of Combustion Oscillations, Flow Turbulence and Combustion, **63**, 395-414.

De Zilwa S R N, Uhm J H and Whitelaw J H (2000) Combustion Oscillations Close to the Lean Flammability Limit, Combust. Sci. and Tech., **160**, 231-258.

De Zilwa, S R N, Sivasegaram, S and Whitelaw, J H (2000) Control of combustion oscillations close to stoichiometry. *Journal of Flow, Turbulence and Combustion,* **63**, 395-414.

Emiris I and Whitelaw J H (2002) Combustion Oscillations Close to the Lean Flammability Limit, Combust. Sci. and Tech., **160**, 231-258.

Emiris I and Whitelaw J H (2003) Control of Combustion Oscillations, Combust. Sci. and Tech., **175,** 157-184.

Emiris, I. and Whitelaw, J. H. (2003) Control of combustion oscillations. *Report to the US Army, May 2002.*

Gibson, M. M. and Launder, B.E. (1978) Ground Effects on Pressure Fluctuations in the Atmospheric Boundary Layer, J. Fluid Mech., **86,** 491-511.

Haworth D C and Pope S B (1986) A Generalized Langevin Model for Turbulent Flows, Phys. Fluids, **29**, 387-405.

Hůlek T and Lindstedt R P (1996) Modeling of Unclosed Nonlinear Terms in a PDF closure for Turbulent Flames, J. Mathematical Computer Modeling, **24**, 137-147.

Janicka J, Kolbe W and Kollman W (1979) Closure of the Transport Equation for the Probability Density Function of Scalar Fields, Journal of Non-Equilibrium Thermodynamics, **4**, 47-66.

Kuan T S and Lindstedt R P (2002) Prediction of Steady and Transient Bluff Body Stabilized Flames, Proceedings of the 6th International Workshop on Turbulent Non-Premixed Flames, http://www.ca.sandia.gov/tdf/Workshop.html.

Kuan T S, Lindstedt R P and Váos E M (2003) Higher Moment Based Modeling of Turbulence Enhanced Explosion Kernels in Confined Fuel-Air Mixtures, Advances in Confined Detonations and Pulse Detonation Engines, Torus Press, pp. 17-40.

Law, C K, Zhu, D L and Yu, G (1986) Propagation and extinction of stretched premixed flames. Twenty First Symposium (International) on Combustion, The Combustion Institute pp. 1419-1426.

Lindstedt R P (1998) Modeling of the Chemical Complexities of Flames, 27th Symposium (Int.) on Combustion, pp. 269-285.

Lindstedt, R P (2003) Private communication.

Lindstedt R P, Louloudi S and Váos E M (2000) Transported PDF Modeling of Pollutant Emissions in Turbulent Jet Flames with Comprehensive Chemistry, 28th Symposium (Int.) on Combustion, pp. 133-139.

Lindstedt R P, Meyer M P and Sakthitharan V (1998) Direct Simulation of Transient Spherical Laminar Flame Structures, EUROTHERM Seminar No. 61 on Detailed Studies of Combustion Phenomena, pp. D5.

Lindstedt R P and Skevis G. (2000) Molecular Growth and Oxygenated Species Formation in Laminar Ethylene Flames, 27th Symposium (Int.) on Combustion, pp. 269-285.

Lindstedt R P and Váos E M (1998) Second Moment Modeling of Premixed Turbulent Flames Stabilized in Impinging Jet Geometries, 27th Symposium (Int.) on Combustion, pp. 957-962.

Lindstedt R P and Váos E M (1999) Modeling of Premixed Flames with Second Moment Methods, Combust. and Flame, **116**, 461-485.

Shih T H and Lumley J L (1985) Modelling of the Pressure Correlation Terms in Reynolds Stress and Scalar Flux Equations, Technical Report FDA-85-3, Cornell University.

Speziale C G, Abid R and Durbin P A (1993) New Results on the Realizability of Reynolds Stress Turbulence Closures, ICASE Report 93-76.

Speziale C G, Sarkar S and Gatski T B (1991) Modelling the Pressure-Strain Correlation of Turbulence: an Invariant Dynamical Systems Approach, J. Fluid Mech., **227**, 245-272.

Zhang S and Rutland C J (1995) Premixed Flame Effects on Turbulence and Pressure-Related Terms, Combust. and Flame, **102**, 447-461.

Zhu M, Dowling A P and Bray K N C (2002) Forced Oscillations in Combustors with Spray Atomizers, ASME Trans., **124**, 20-39.